CRANFIELD UNIVERSITY

Nicholas Brocklesby

Screening of Copper Based Particles Supported on Bentonite for Chemical Looping with Oxygen Uncoupling

School of Energy, Environment and Agrifood
Carbon Capture and Storage

MSc by Research

Supervisors: Professor Vasilije Manovic

Professor Edward Anthony

2016

CRANFIELD UNIVERSITY

School of Energy, Environment and Agrifood
Carbon Capture and Storage

MSc by Research

Nicholas Brocklesby

Screening of Copper Based Particles Supported on Bentonite for Chemical Looping with Oxygen Uncoupling

Supervisors: Professor Vasilije Manovic

Professor Edward Anthony

2016

This thesis is submitted in partial fulfilment of the requirements for the degree of MSc by Research

ABSTRACT

The vast majority of the scientific and political communities agree that the release of greenhouse gases from anthropogenic sources is leading to an increase of global average temperature. One of the main gases involved in this effect is carbon dioxide (CO_2). International scientific and governmental bodies such as the IPCC agree that CO_2 release must be reduced and targets for the reduction of the amounts of gas that are released have been ratified by national governments across the world. One of the largest sources of anthropogenic CO_2 is the combustion of fossil fuels for electricity production.

Several methods of capturing the CO_2 produced by combustion have been developed, with chemical looping combustion (CLC) being suggested by the IPCC as a promising method to achieve the targets in reducing the release of this gas. The combustion of solid fuel in a CLC reactor is not reasonable without modification of the process and chemical looping with oxygen uncoupling (CLOU) is the most promising method of achieving this goal.

The CLC process use oxygen carriers to transport oxygen from the air to the fuel in a separate chamber for combustion. CLOU is a form of CLC where the oxygen carrier releases gaseous oxygen. The development of suitable oxygen carrier materials is important in order to progress CLC and CLOU to usable industrial scale technologies and much research has been done into developing them. One of the most widely studied oxygen carrier materials for CLOU is copper oxide supported on magnesium aluminate, however it has been found that this material degrades over many redox cycles, giving the particles a short usable lifetime.

This study aims to determine the potential of a different material, with a long usable lifetime, for use in CLOU systems. This material again uses copper oxide, but now supported on bentonite and produced by mechanical mixing and pelletisation. This material is tested in terms of its initial characteristics consisting of crystalline phases determined by XRD, crushing strength and SFEG imaging. The ability of the material to be reduced in an inert environment, and oxidised in air has also been tested in a fluidised bed. The material was subjected to multiple

reduction and oxidation cycles and the characteristics will be tested again. The study has endeavoured to determine if the material meets the requirements of oxygen carriers in terms of reducibility and oxidisibility, and whether the material maintains these characteristics over many redox cycles.

The results of this study indicate that bentonite acts as a tough support for CuO particles, able to withstand use in a fluidised bed without significant attrition. XRD results show that the particles designated Cu60B40 actually contained the highest amount of CuO of all particles produced, despite having the smallest proportion of CuO added during production. Fluid bed testing shows that the Cu60B40 particles were also able to give off the most oxygen during CLOU testing. These results combine to indicate that sintering occurred in the particles containing the least amount of support, and that the support phase is necessary to maintain oxygen carrier performance, which is in line with previous research.

TGA testing with reducing gas showed a much higher degree of conversion than the fluid bed testing in all samples. This indicates that these copper oxide-bentonite particles are better suited to use with gaseous fuels than to solid fuel.

This study has followed on from work such as Tian et al(2008) and Arjmand, M. et al (2013) in looking at copper based particles, but takes a more fully rounded approach looking at both reduction in reducing gas, and in inert atmosphere, as well as performance while fluidised. This has shown unexpected pitfalls in oxygen carrier selection. In order to find copper based particles that are better suited to CLOU activity, it is suggested that further work be carried out into the use of cement as a support phase. It is important to retain the full range of tests carried out here to rigorously test these particles.

Keywords:

Chemical Looping Combustion, Fluidised Bed, Carbon capture and storage, Oxygen carrier, Combustion

ACKNOWLEDGEMENTS

I wish to thank both Professor Vasilije Manovic and Professor Edward Anthony for their assistance in progressing this project. I also with to thank Kumail Haider, Dawid Hanak and Maria Erans Moreno for their support and advice in progressing this project. I also wish to thank contributors from Imperial College London, Professor Paul Fennel and Dr John Blamey, for their assistance with TGA testing.

TABLE OF CONTENTS

LIST OF FIGURES

LIST OF Tables

LIST OF EQUATIONS

LIST OF ABBREVIATIONS

OC	Oxygen Carrier
FR	Fuel Reactor
AR	Air Reactor
CLC	Chemical Looping Combustion
CLOU	Chemical Looping with Oxygen Uncoupling
iGCLC	In-situ Gasification Chemical Looping Combustion
ASU	Air Separation Unit
GHG	Green House Gas
SFEG	Field Electron Gun Scanning Electron Microscopy
SEM	Scanning Electron Microscopy
XRD	Xray Diffraction
TGA	Thermo-gravimetric Analyser

1 Introduction

1.1 The Basis of the need for Carbon Capture and Storage

The Intergovernmental Panel on Climate Change 4th Assessment Report (2007) shows that there is a large body of evidence to indicate that global average temperatures are rising. Greenhouse gases, or GHGs occur naturally in the atmosphere, however the concentration of these gases, particularly CO_2 is rising (Bernstein et al., 2007). It is this increase in GHG concentration which is believed to be the cause of the rise in global temperatures. The increase in concentration of CO_2 is not natural, but is driven by the release of this gas from anthropogenic sources. Major anthropogenic sources of CO_2 include transport, industrial manufacture such as concrete production, and electricity production from the burning of fossil fuels (Bernstein et al., 2007).

There has been a concerted international effort to introduce global measures to reduce the amount of anthropogenic CO_2 released into the atmosphere. The United Nations Framework Convention on Climate Change (UNFCCC) in 1998 adopted the Kyoto Protocol. This introduced targets to reduce emissions of CO_2. The UK has also passed the climate change act in 2008, which set a legal obligation to reduce CO_2 emissions by 80% by 2050.

In order to meet this target, electrical power generation must be achieved with reduced CO_2 emissions. The UK government has been committed to introducing and expanding green energy technologies such as wind power, tidal power and solar power generation. Nuclear power generation is also to be increased. These alternative sources of electrical power will have an effect on CO_2 emissions, however it is predicted that electricity demand will increase in the future and fossil fuel powered production will remain a major factor in power generation. Due to this, the concept of capturing CO_2 and storing it, most likely in geological

formations (Riley 2010) to prevent release into the atmosphere, has been pursued.

2 CO_2 Capture strategies

2.1 Post-combustion Capture

Post-combustion CO_2 capture methods are able to be retrofitted to existing power plants, and are based around absorption, adsorption, membrane and cryogenic separation. It has been argued that the most promising of these options is chemical absorption, primarily by an amine such as monoethanolamine (Yu et al., 2012). However this method suffers from several drawbacks including the degradation of the sorbent by SO_2, NO_2 and O_2, and the need for an energy intensive regeneration step which significantly reduces the efficiency of the power plant equipped with amine scrubbing (Wilcox 2012).

2.2 Pre-combustion Capture

Pre-combustion capture involves removal of carbon containing gases prior to combustion (Wilcox 2012). Solid fuel is gasified producing a mixture of CO and H_2 gases, known as syngas. This can then be shifted via the water gas shift reaction shown in Eq 2.1.

$$CO + H_2O \leftrightarrow CO_2 + H_2 \qquad \text{Eq 2.1}$$

The CO_2 is then removed via absorption or membrane as with post combustion capture, however the CO_2 partial pressure is much higher, making the separation easier. This process suffer from the need for an air separation unit, or ASU which cryogenically removes O_2 from air, providing a pure O_2 stream.

2.3 Oxyfuel Capture

Oxyfuel capture involves combusting fuel in a near pure O_2 environment (Wilcox 2012). A stream of oxygen is provided from an ASU instead of combusting fuel in air, with the high nitrogen content involved. This significantly reduces NO_x content in the flue gas and gives almost entirely CO_2 and H_2O as the only products of combustion. The H_2O can be condensed out from the flue gas to give a near pure stream of CO_2 ready for compression and sequestration. This process also requires an expensive ASU, increasing the cost per unit of electricity produced.

2.4 Chemical looping Combustion

Oxyfuel capture requires the separation of oxygen gas form air using an ASU. It has been proposed that oxygen can be supplied to the fuel for combustion from the air via a different method from an ASU. Chemical Looping combustion is a technology first developed by Lewis, Gilliland and Sweeney who published a paper in 1951 outlining chemical looping combustion. (Lewis et al., 1951). The process transports oxygen from the air to the fuel reactor to facilitate combustion of the fuel. This operates by means of a metal which can be oxidised by air in the air reactor (AR) to form a metal oxide, which is transported to the fuel reactor (FR) and must be able to oxidise the fuel. The flue gas from the fuel reactor consists entirely of CO_2 and H_2O, just as with oxyfuel combustion and gives inherent CO_2 capture. As the CLC approach uses a metal oxide as the transport medium for oxygen it differs fundamentally from oxyfuel systems and is essentially a new form of fuel conversion technique. CLC is considered a compelling option for CO_2 capture because the cost per tonne of avoided CO_2 has been estimated at 6 – 13€ for CLC, 18 - 37€ for pre-combustion capture technology using IGCC and 13 - 30€ for oxyfuel combustion(Adanez et al., 2012). Additional estimates place the cost in the range 14 – 72$ per tonne of avoided CO_2 for oxyfuel and 37 – 75$ per tonne of avoided CO_2 for MEA capture.(Bernstein et al., 2007)

3 Principles of Chemical Looping Combustion and Chemical Looping with Oxygen Uncoupling

3.1 Process fundamentals for CLC

CLC is a novel fuel conversion technique, which removes the need for a CO_2 separation step as there is no direct contact between the fuel and air. As mentioned above, CLC makes use of a metal oxide to transport the oxygen needed for combustion from air to the fuel. For this reason the metal oxide is referred to as oxygen carrier (OC). The most commonly envisioned design for a CLC reactor consists of 2 interconnected fluidised beds. Oxidation of the OC takes place in a chamber known as an air reactor (AR) and proceeds by Eq 3.1.

$$(2n+m)Me_xO_{y-1} + (n+m/2)O_2 \rightarrow (2n+m)Me_xO_y \qquad \text{Eq 3.1}$$

The OC is then transported to the fuel reactor (FR), where it oxidises the fuel via Eq 3.2

$$(2\mathrm{n}+\mathrm{m})Me_xO_y + C_nH_{2m} \rightarrow (2n+m)Me_xO_{y-1} + nCO_2 + mH_2O \qquad \text{Eq 3.2}$$

The flue gas from the AR consists of air with reduced oxygen content. The flue gases from the FR consist of CO_2 and H_2O, and after condensation of H_2O, a pure CO_2 stream is achieved. The design based on 2 interconnected fluidised beds relys on loop seals to avoid gas leakage from 1 reactor into the other. Leakage would result in reduced CO_2 capture efficiency from CO_2 leaking into the AR and being released into the atmosphere. It would also lead to a less pure CO_2 stream for sequestration from air leaking into the FR. A basic schematic view of this reactor set up is given in Figure 3.1.

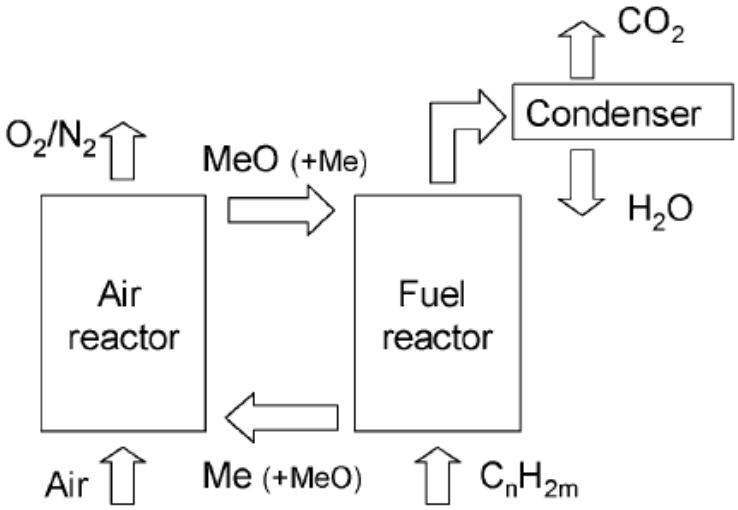

Figure 3.1 Basic schematic view of a CLC plant showing the air reactor and fuel reactor.

3.2 Operating a CLC plant using solid fuel

3.2.1 In-situ Gasification Chemical Looping Combustion

Coal has been a leading source of power for electrivity production over the past few years and has risen to be the most used fuel, and its use is continuing to rise (Hemingway & Michaels 2012). In terms of use of solid fuel in a CLC based system, the reaction of the solid OC with the solid fuel is not appropriate due to the slow nature of this solid – solid reaction and as such there are a number methods which have been developed to use solid fuel. The 2 most significant methods which have been most intensely studied are covered here. The first is known as In-situ Gasification Chemical Looping Combustion (iGCLC) and involves gasification of the solid fuel by reaction with CO_2 or H_2O to give syngas composed of CO and H_2 (Cao & Pan 2006). These gases are then able to react with the oxygen carrier as in normal CLC. However the gasification step is the slowest and therefore rate limiting step, which will have a significant effect on the rate that fuel is converted. There is also the threat that unburnt char could be circulated into the AR and cumbust normally in the air, meaning that CO_2 is

released from the AR and reducing the overall CO_2 capture efficiency (Berguerand & Lyngfelt 2008).

3.2.2 Chemical Looping with Oxygen Uncoupling

Chemical Looping with Oxygen Uncoupling (CLOU) is the second method. This method depends on the additional property of a small number of metal oxides to enable use of solid fuel in the FR. This property is the release of gaseous oxygen at high temperature. There are 3 metal oxides which have been identified as showing this behaviour and which are able to achieve high fuel conversion. These are; CuO, Mn_2O_3 and Co_3O_4. These metal oxides will release oxygen up to a particular partial pressure of O_2 which varies between the metal oxides and with temperature. Figure 3.2 shows the equilibrium partial pressures of O_2 at the surface of these metal oxides at different temperatures.

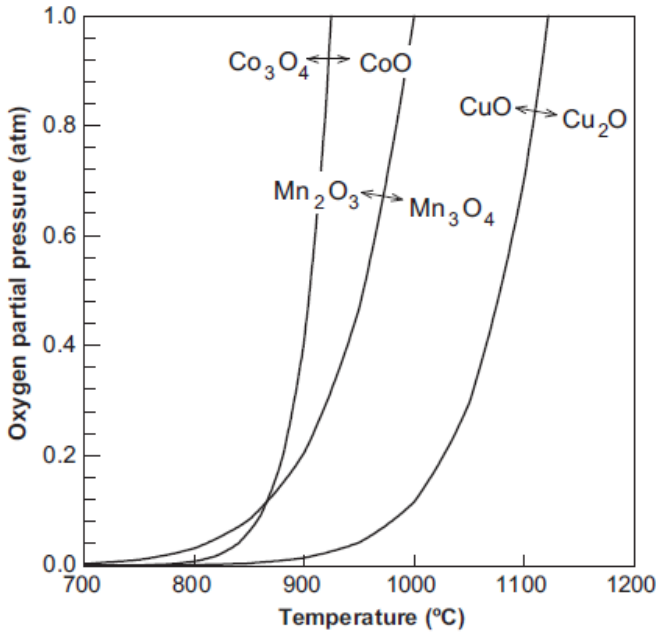

Figure 3.2 The equilibrium partial pressure of oxygen at the surface of 3 metal oxides plotted against temperature. (Image from Adanez et al., 2012)

This property means that, while the metal oxides will release oxygen in a low oxygen FR environment, the temperature in the AR must be kept low enough that the partial pressure of oxygen is above that at equilibrium for the metal used. Here the CuO/Cu_2O system allows for the highest AR temperature. The oxygen concentration in the OC environment has also been shown to have a strong effect on the rate of oxidation and reduction reactions. The difference between the OC environmental O_2 partial pressure and equilibrium partial pressure is suggested as the driving force for these reactions (Adánez-Rubio et al., 2014). The CuO/Cu_2O system will also have the lowest release rate of O_2 in the FR at a given temperature compared to the Mn_2O_3/Mn_3O_4 and Co_3O_4/CoO systems; however the O_2 will be consumed by fuel combustion, offsetting this factor. Equations 3.3 – 3.5 show the oxygen release reactions with enthalpy changes for CuO/Cu_2O Mn_2O_3/Mn_3O_4 and Co_3O_4/CoO systems.

$$4CuO \rightarrow 2Cu_2O + O_2\ \Delta H_{850^oC} = 263.2\ kJ/mol\ of\ O_2$$ Eq 3.3

$$6Mn_2O_3 \rightarrow 4Mn_3O_4 + O_2\ \ \Delta H_{850^oC} = 193.9\ \ kJ/mol\ of\ O_2$$ Eq 3.4

$$2Co_3O_4 \rightarrow 6CoO + \ O_2\ \Delta H_{850^oC} = 408.2\ \ kJ/mol\ of\ O_2$$ Eq 3.5

This shows that the release of oxygen for all systems is endothermic, and that the manganese system is the least endothermic.

Figure 3.3 gives a visual representation of the processes involved in the fuel reactor in iGCLC and CLOU plants.

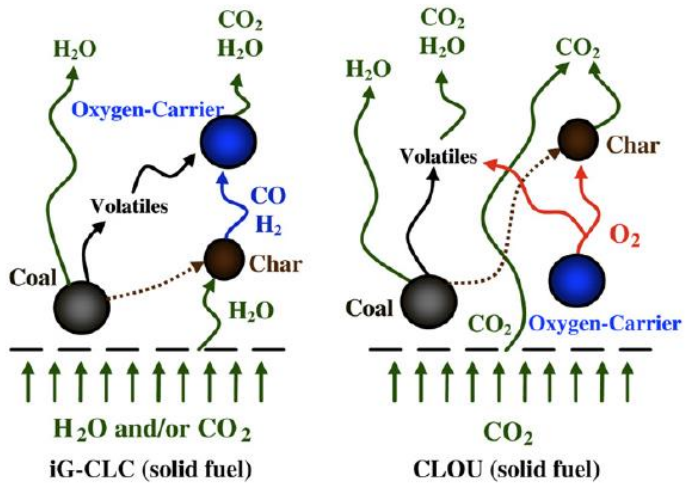

Figure 3.3 The main processes involved in the fuel reactor in an iGCLC and CLOU plant. (Adanez et al., 2012)

4 Main Factors for effective design of a CLOU or CLC plant

4.1 Particle Characteristics

The oxygen carrier particles are intrinsic to CLC and CLOU plants. There are a number of key characteristics which are required of oxygen carrier particles (Adanez et al., 2012), these are:

- The thermodynamic characteristics in the FR must be favourable to give high conversion of the fuel.
- The OC particles should give high reactivity in oxidation and reduction and this should be maintained over many redox cycles.
- The particles must show high resistance to attrition to minimise the loss of fine particles from the system.
- The particles should not show a tendency to agglomerate, allowing the maintenance of fluidisation.
- Sufficient oxygen carrying capacity. The particles must be able to deliver enough oxygen to the FR from the AR to enable complete conversion of the fuel.
- The production and disposal of particles should not be harmful to the environment.
- The cost of the particles should be kept to a minimum and be competitive with other methods of achieving CCS.
- Carbon deposition should not occur on the carrier as this would lead to carbon combustion and release of CO_2 in the AR.

Work has been done into many metal/metal oxide systems to determine the feasibility of their use for CLC (Jerndal et al., 2006). It was found that Fe_2O_3, CuO, NiO and Mn_2O_3 showed appropriate thermodynamic properties and

gave good reaction rates for fuel conversion of at least 0.99. As such these metal oxides have been studied for use as active component in OCs.

Studies have shown that use of particles which are unsupported show high attrition and loss of reactivity over progressive cycles. This can be prevented by the use of support material. This support improves the attrition and agglomeration resistance of the particles and improves the maintenance of the oxidation and reduction properties of the active metal oxide over many redox cycles (De Diego et al., 2004).

Oxygen carrying capacity is a product of the amount of oxygen supplied in the FR per unit mass of active metal oxide, and the active to support phase ratio in the OC. It is defined by Eq 4.1.

$$R_{OC} = \mathrm{x}_{OC} R_A \qquad \text{Eq 4.1}$$

$$R_A = (m_o - m_r)/m_o \qquad \text{Eq 4.2}$$

In Eq 4.1 R_{OC} is the oxygen carrying capacity of the OC, x_{OC} is the weight ratio of the active phase to support phase, R_A is the oxygen carrying capacity of the active phase of the OC. Equation 4.2 gives the definition of the oxygen carrying capacity of the active phase of the OC. Here m_o is the mass of the active metal oxide when fully oxidised and m_r is the mass of the active metal oxide when fully reduced. Figure 4.1 indicates oxygen carrying capacity for a range of active metal oxides. Maximising oxygen carrying capacity involves choosing an active metal oxide with a high carrying capacity and using a high active to support phase weight ratio in the OC.

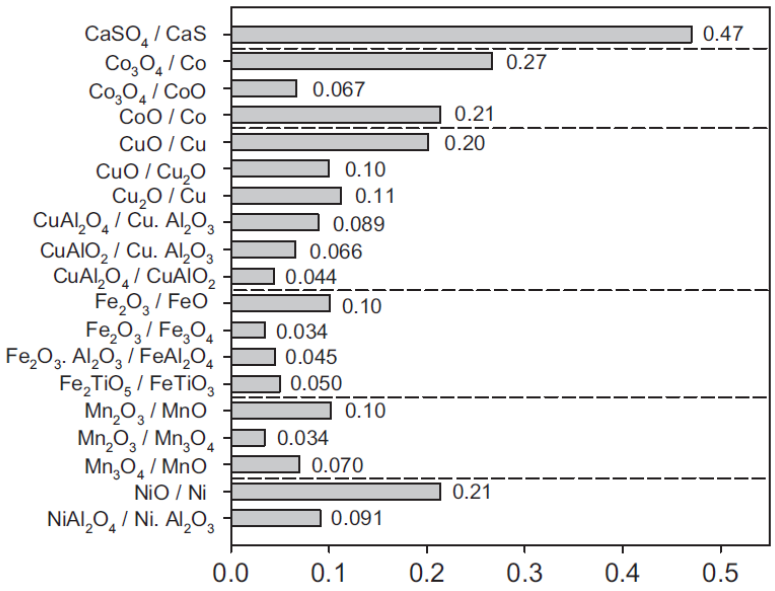

Figure 4.1 Oxygen carrying capacity for active metal oxides (R_A). (Adanez et al., 2012)

The cost of oxygen carrier particles is based on the cost of the OC, OC production costs and OC disposal costs. The other major factor in cost is the make-up flow of new OC particles required (Abad et al., 2007). Because of this, particles which will remain usable over many redox cycles are necessary.

Carbon deposition has been investigated and can happen when there is a low amount of oxygen available in the FR. The amount of oxygen needed for this to happen is below the stoichiometric amount of oxygen required for complete fuel conversion. This situation should not occur in an adequately operating plant, and has not been found in fluidised bed tests which have been carried out (Jerndal et al., 2006), (Abad et al., 2007).

Additionally to the factors mentioned above, the active phase must not react with from the inert phase of the material. Some active/inert combinations have been shown to react with each other to form unreactive complexes (Imtiaz et al., 2014).

This uses up active material and reduces the oxygen carrying capacity of the particles. This phenomenon is dependent on the active/support combination and can be solved using additives which selectively form spinel compounds with the support phases, preventing the active phase from interacting with the support.

4.2 Oxygen Carrier Particle Production Methods

There are several methods of preparing oxygen carrier particles for use in CLC and CLOU. The most studied of these will be discussed here. First it is worth noting that all methods end with a calcination step which can be performed over a range of temperatures. This step hardens the particles and gives them better ability to hold together as a solid, discreet particle. Higher calcination temperatures give higher crushing strengths but reduce surface area.

Mechanical mixing is a method where powders of the active and inert metal oxides can be purchased directly for use in the particles. The powders are physically mixed together, e.g. in a ball or shear mill. A binder may be added to hold the powders together until calcination. The desired size particles can then be obtained by crushing and sieving the particles. These particles a range of crushing strengths which vary with support used (Gayán et al., 2012; Zhou et al., 2014), but have been shown to experience high attrition (De Diego et al., 2004). They can also result in uneven distribution of inert and support throughout the particles (Chuang et al., 2008). They have been shown to give acceptable reactivity (Zhou et al., 2014).

Pelletisation is a variation of mechanical mixing, where mixing occurs in a bowl. There are 2 blades in the bowl, the first is a large blade at the bottom of the bowl called the agitator which rotates at 500 rpm, the second is a smaller blade at the side called the chopper which rotates at 2500 rpm. This method has been shown

to produce particles with good attrition resistance and reactivity (Wu et al., 2012). The method also avoids additional cost and time spent on more complex methods described below.

Impregnation involves using a powder of the required support, and soaking this in a solution of a nitrate of the active metal. The active metal oxide is then obtained by thermal decomposition of the nitrate. The mixture is then dried and calcined and correct particle size is achieved by crushing and sieving. A high level of active metal oxide loading is harder to achieve and the process must be repeated go reach compositions of active metal oxide as high as other methods (Gayán et al., 2012). These particles give a range of crushing strengths, varying with support material (De Diego et al., 2004), however an additional study (Chuang et al., 2008) determined that they give particles with active metal oxide covering the exterior of larger support particles, which they suggested led to agglomeration.

Coprecipitation involves dissolved molecules of the required metals, generally metal nitrates are used. In this case nitrates of the active and support phases are mixed together in solution. An additive is used to precipitate the metals out of solution together. The precipitate is then thermally decomposed to their metal oxides. The mixture is then dried, calcined and crushed to size. This process has been shown to give particles with poor qualities when used with CuO (Chuang et al., 2008). These qualities could be enhanced by increasing the pH of the nitrate solution. The study headed by Chuang et al (Chuang et al., 2008) also found that by adding sodium carbonate, the solute precipitated out as copper carbonate and aluminium hydroxide. These were then thermally decomposed to give the metal oxides. These particles were found to have good crushing strength and attrition resistance and, no agglomeration tendency as well as good reactivity which was stable over repeated reduction and oxidation cycles.

The sol gel method has also been developed to produce oxygen carriers. In this method a trialkoxide is used as precursor, eg $Al(OC_3H_7)_3$. Using the Yoldas

process then gives a boehmite sol. A metal nitrate solution is then added in the concentration to give the required loading of metal. This is then thermally decomposed to produce the metal oxides for the OC. The product is then crushed and sieved to size and calcined (Hai-bo et al., 2008).

Freeze drying is a process defined by the drying of the particles. Metal oxide powders are purchased in fine powder form. These are mixed together in the same way as with mechanical mixing, with water added. They are then pumped through a spray nozzle into liquid nitrogen where they freeze instantly. The particles are then placed in a freeze drier with pressure at the water vaporisation pressure for the given temperature below O ^{o}C. the resulting particles are then calcined. This produces particles with good sphericity to give enhanced fluidisation properties. This process requires a supply of liquid nitrogen, which is unlikely to be appropriate for large scale production (Jerndal et al., 2010).

Spray drying is another method that has been widely investigated. This method involves a similar preparation stage to freeze drying, where powders are mixed in a mill with a binder to ensure the particles stay together before calcination. The mixed wet material is then pumped through a spray nozzle to be dried by passing through air. This method has been shown to give particles with good oxidation and reduction reactivity.

5 Literature Review

Several metals have been studied as they show desirable properties for use in CLC. Iron, nickel and copper have been the subject of the most research and will be discussed here. Fe based materials were found to show generally good reactivity with syngas, but not with methane. Fe based OCs also have an inherently low oxygen transport capacity (Abad et al., 2007). This is due to the limitation of the oxides of iron that are suitable for use in CLC. A study by E. Jerndal (Jerndal et al., 2006) found that only reduction from hematite to magnetite (Fe_2O_3 – Fe_3O_4) is appropriate for use in CLC. Reaction to lower oxidation states of iron results in a significant drop in the possible conversion of fuel. Lastly, significant properties in favour of the use of iron based carriers are that they are non-toxic, unlike the other possibilities such as Ni, and to a lesser extent, Cu, and it has a relatively low price compared to those same other metals. Nickel also shows promise for use in CLC. The study by Jerndal et al shows that nickel cannot reach full conversion of fuel as iron or copper based OCs can, but it is able to reach conversion of 0.98, which is extremely high. The reactivity of Ni based OCs is high with all fuel types (Jerndal et al., 2010). Nickel also has a relatively high oxygen carrying capacity, meaning lower solid circulation rates required in the plant. Copper has been the subject of a large body of research due to its aptitude for CLOU. One major drawback of copper oxides for use in this area is their low melting point and tendency to agglomerate and defluidise (Adánez et al., 2006). Copper based OCs show good reactivity (Adánez-Rubio et al., 2011), however they can show a range of crushing strengths based on the support phase used (De Diego et al., 2004) Copper is able to reach complete conversion of fuel (Jerndal et al., 2006) but cannot be disposed of as easily as iron due to its toxicity.

There are a number of materials that have been previously selected and tested in many studies for use as inert support in the OC particles. These materials

include Al_2O_3, ZrO_2, SiO_2, TiO_2 and sepiolite. These materials will have a particular interaction with each active metal used in the OC (Mattisson et al., 2007). A study by Adanez-Rubio et al (Adánez-Rubio et al., 2011) examined different support materials and particle production methods including wet impregnation and mechanical mixing. They studied alumina, magnesium aluminate, sepiolite, zirconia, silica, magnesia and titania as supports. They found that samples prepared on titania and alumina had low reactivity. The low reactivity of alumina supported copper OCs has been attributed to the formation of copper aluminate which is less reducible than CuO. They also found that magnesia interacted with CuO, reducing its reactivity. In fluidised bed tests they found agglomeration problems with many supports. Magnesium aluminate did not show agglomeration problems, and zirconia with 40% CuO content did not show agglomeration problems. Zirconia supported particles showed low solid conversion and low O_2 concentration in fluid bed tests. Magnesia aluminate samples showed high attrition in these tests and new samples were prepared increasing calcination time and temperature significantly which gave a lifetime of around 500 hrs. An additional study (De Diego et al., 2004) agreed with these results, but showed that by using coprecipitation this support could give better crushing strengths with fresh samples.

Another study by Adanez-Rubio et al (Adánez-Rubio et al., 2012) shows that CuO active phase supported on $MgAl_2O_4$ prepared by spray drying was able to achieve very good oxidation and reduction performance, and to maintain that performance over prolonged use. However when tested in a 1.5 kW continuous fluidised bed reactor, the particles experienced attrition and the reactor had to be shut down after 40 hrs due to loss of fine particles. This was associated with a drop in the crushing strength of the particles from 2.4 N for fresh particles to 0.6 N for particles used in the continuously operated reactor. The drop in crushing strength was attributed to porosity increasing from 16.1% to 40.3% for fresh and used particles respectively.

A study by Corbella (Corbella et al., 2006) found that particles based on copper supported by silica did not experience large changes in porosity over repeated redox cycles. This could indicate that these particles would be able to resist attrition in larger continuously operated facilities.

A study by de Diego (De Diego et al., 2004) indicates that particles of copper prepared with titania and zirconia by mechanical mixing were unable to reach full conversion in the air reactor, meaning the oxygen carrying capacity of these particles would be reduced. Alumina has been extensively studied as a support material for copper based particles for CLOU (Imtiaz et al., 2014; Chuang et al., 2008; De Diego et al., 2004). Studies have shown that there is a detrimental interaction of copper with the alumina (Imtiaz et al., 2014). For this reason magnesium oxide is added, forming $MgAl_2O_4$ complexes. This is shown to reduce the degree of CuO which interacts with Al_2O_3 and allows higher CuO content and higher oxygen carrying capacity. Additionally, these particles are shown to exhibit higher attrition resistance and resistance to chemical degradation. This is shown by higher and more consistent solid conversion ratios over many oxidation/reduction cycles. A study by Gayan et al (Gayán et al., 2012) studied similar particles to these prepared by impregnation, but determined that it was too time consuming to achieve sufficiently high proportions of active phase to inert phase, and so sufficiently high oxygen carrying capacity. For this reason it was deduced that impregnation is not an appropriate preparation method. When zirconia goes through crystal structure transitions, the density and unit cell volume changes, this causes fracturing of the material and is believed to cause attrition in particles supported by this (Rydén et al., 2014). This study also found that copper supported on CeO_2, ZrO_2 and on yttrium stabilised zirconia produced by spry drying showed good reactivity in conversion of fuel, but high attrition.

Studies focusing on CLOU with CuO/Cu_2O suggest that particles supported on $MgAl_2O_4$ show the best combination of reactivity and durability, some samples supported on zirconia have also shown acceptable reactivity and can show good

attrition resistance if used with low active phase content. Spray drying has been the main focus of continued study, with magnesia aluminate most commonly used as support. However these studies have shown that attrition is a problem with prolonged use of these particles.

Bentonite has been studied as a support material by several studies. Manovic et al (Manovic & Anthony 2009) found that bentonite could produce sintering effects in calcium based sorbent particles. However, bentonite has been used with some success as a support for nickel (Tian et al., 2009). Bentonite has also been investigated as a support for copper based oxygen carriers (Tian et al., 2008), (Monazam et al., 2012). The study by Monazam et al investigated bentonite as a support for copper particles produced by coprecipitation and found reasonable performance of particles. Tian et al (Tian et al., 2008) studied bentonite as a support for copper particles produced by mechanical mixing. They found that the particles achieved a good degree of conversion and showed stable performance over 10 cycles.

6 Research Proposal

6.1 Research Aims

The goal of this study if to produce and test an oxygen carrier with good performance in terms of reactivity, oxygen carrying capacity and crushing strength, and is able to maintain this performance over many redox cycles. This oxygen carrier must be produced using a simple method that can be scaled up. The focus of this study will be around particles for use in the CLOU process. The proposed particles will utilise CuO as the active phase in the OC. Much research has gone into finding suitable support material for an OC based on this material and it has been determined that magnesium aluminate shows promising signs of being a good support phase for this type of OC. However it has been noted that

this material will deteriorate over many redox cycles. It has therefore been decided that more work is necessary into finding another support phase. In previous studies, mechanical mixing has shown relatively poor results, however it is accepted that this method is the easiest and cheapest to scale up. The production method will therefore consist of a variation of this method, which has shown promising results, known as pelletisation. The support that will be tested is bentonite.

Bentonite is a natural clay, which is widely available and has a large number of uses, from cosmetics to sealants, to drilling. The composition varies as with other natural materials, but consists primarily of alumina and silica, with small amounts of CaO, MgO, K_2O, Na_2O, and S. Bentonite is formed of lamellar platelets with water between each platelet. Each platelet is formed from 3 layers, a central octahedral alumina layer with 2 tetrahedral silica layers either side. The aluminium and silicon ions can be substituted by lower valence metals. This causes a change in charge, which is addressed by exchange in cations, primarily calcium and sodium. The prevailing presence of either sodium or calcium has implications on the amount of water, which can be absorbed by the clay. A prevalence of sodium cations results in a greater capacity for water absorption. The sodium cation allows more water to penetrate between the platelets. Calcium cations (Ca^{2+}) have a stronger positive charge than sodium cations (Na^{+}) and will not allow water to penetrate the platelets, leading to lower absorption capacity.

These particles will be characterised using an array of standard characterisation techniques. After this, the particles will undergo testing to investigate their ability to release gaseous oxygen in an inert environment. Finally, the particles will be subjected to redox cycles using fuel gas in the reducing stage. During these cycles, the particles' ability to convert the fuel gas will be investigated. These samples will then be characterised as the fresh particles were.

The formal aims of the study are;

- To prepare particles using CuO as active phase and bentonite or alumina cement as support.
- To establish characteristics of the freshly produced particles by measuring porosity, crushing strength, establishing crystal phases using XRD.
- To complete many reduction and oxidation cycles using a fluid bed furnace. This will indicate the resulting particle's ability to achieve combustion of fuel and reveal the composition of the gases evolved from this.
- Retest the particles characteristics after redox cycles to establish how they change with prolonged use. This will indicate how sintering affects the particles and their resistance to sintering and possible attrition.

7 Methodology

7.1 Research Method

This study will produce OC particles using bentonite as support and using CuO as the active phase. The particles will be prepared by mechanical mixing and preparation by a pelletiser. This process does not involve large quantities of waste material or dangerous waste products that would need to be processed. This also allows reasonably high active phase loading. The fresh particles will undergo several tests to determine their initial characteristics. This series of tests will involve XRD characterisation to determine the presence of active phase. It will involve crushing strength tests and finally porosity tests.

The particles will then pass through 2 stages of testing. The first stage will be the oxygen release/ oxidation testing. This will utilise a fluid bed and will switch

between cycles of reduction in an inert atmosphere, and oxidation. Initially the particles will be loaded into the chamber and fluidised by pure CO_2. The equipment will heat up to 880^oC and the concentration of oxygen in the off gas will be measured. After 6 minutes, the gas will be switched to 5%oxygen, 95% nitrogen mix. The oxygen concentration will again be measured to show that oxidation is occurring and when it stops. This is the end of testing at that temperature, and the temperature will be increased to 900^oC. The gas will then be cycled to CO_2 again for 4 minutes and then back to the oxygen/nitrogen mix. This cycle will then be carried out again at 920^oC and 940^oC. This test will indicate firstly that the samples are capable of CLOU behaviour, and secondly what the rates of oxygen release and oxidation are for these particles.

The next stage of testing will consist of cycles of reduction and oxidation in a TGA with carbon monoxide used in the reduction stage. The cycles will take place at 940^oC, 920^oC, 900^oC, and 880^oC using a 5% oxygen/ 95% nitrogen mix during oxidation, and a CO/ nitrogen mix during reduction. The distinction between this test and the prior test will be that this test cannot show CLOU behaviour, but will show the behaviour of the particles in this environment. The particles will also be exposed to a more realistic cycle of oxidation and reduction, with heat release in the reduction stage. The TGA equipment used is depicted in Figure 7.1a. The fluid bed stage of testing will be carried out in the equipment shown in Figure 7.1b.

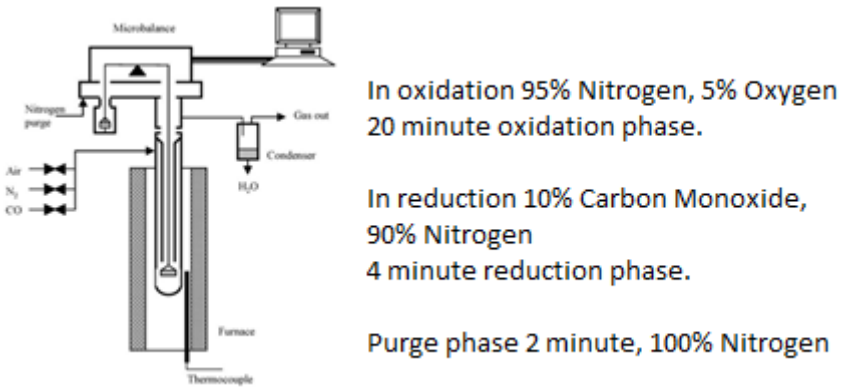

Figure 7.1a setup of TGA to be used. (de Diego et al., 2004)

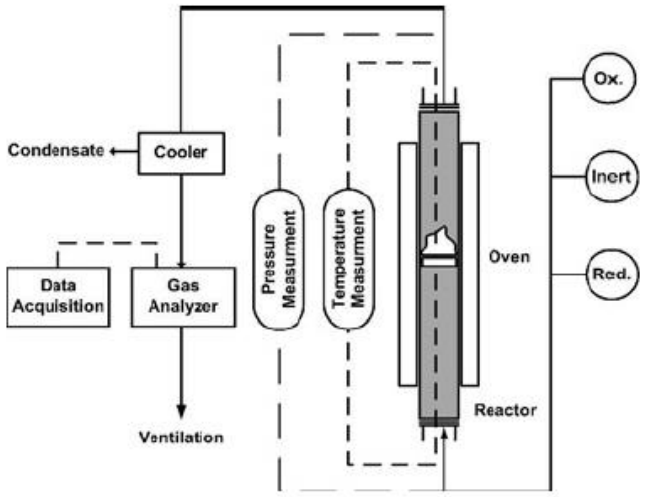

Figure 7.1b Set up of the furnace to be used. (Arjmand et al., 2013)

7.2 Particle Production

Oxygen carrier particles were produced using copper II oxide as the active phase and bentonite powder, obtained from Mistral Chemicals, as the support phase. The copper II oxide was also acquired as a fine powder. For this project, 3 batches of oxygen carrier particles were produced. A pelletizer was used to produce particles from the raw ingredient powders, the model of pelletizer used was a Glatt TMG 1/6, using a 4 L vessel. (Wu et al., 2012) used the pelletisation method to create particles for study. They found that optimal pelletisation required specific speeds of the blades in the pelletisation chamber and the amount of water droplets added.

The initial batches of production were carried out with 1 kg of raw ingredients. These first batches gave very poor yield of particles. Much of the material stuck to the side of the chamber or formed large clumps. These batches were used to

develop a procedure for producing particles around 1 mm in size with acceptable yield. The granulator, a Glatt TMG 1/6 unit, consists of a large standing base unit which provides power via 2 spinning shafts to a 4 L vessel. This vessel contains 2 large spinning blades connected to a shaft at the base, known as the agitator. These blades are 10 cm long and 3 cm wide. There are also 4 smaller blades mounted to the side of the vessel, known as the chopper. The chopper blades are 4 cm long and 1 cm wide and are angled at 50^{o} into the vessel. Each batch used 1 kg of material. The process started with short bursts with the agitator spinning at 150 rpm and the chopper spinning at 1000 rpm for 20 seconds. This was then increased the speeds to 250 rpm for the agitator and 1750 rpm for the chopper for 20 seconds. This was then increased the speed again to 400 rpm for the agitator and 2000 rpm for the chopper in 10-second bursts. Around 10 ml of water was added during each burst. Bentonite will absorb a significant amount of water. Because of this, pelletisation continued until the particles had reached approximately 1 mm in diameter. The size of the particles was checked with a sieve and additional 10 second bursts were added if the size was found to be too small.

Pelletisation of these particles occurred most abruptly at high blade speeds. The bursts with low blade speed ensured good mixing of the constituent powders and that all of the mixture was wet. The amount of water added was controlled finely as too much would lead to formation of large clumps with no small particles. The short bursts at high blade speeds were necessary as the particles formed very quickly and would grow too large with any longer bursts. The following batches were produced with 0.5 kg of raw material at a time, with undersized particles being reprocessed.

In total, 304 g of CuO60B40, 277.5 g of CuO80B20, and 413 g of CuO90B10 were produced. Immediately out of the pelletiser, the particles were soft and the bentonite had absorbed a lot of water. In order to improve the hardness of the particles they were calcined. The calcination took place at 900^{o}C

for 6 hours in a furnace. After calcination, the particles were much harder and had shrunk to around 50% of their size before calcination. These effects are due to loss of the water that the bentonite had absorbed during pelletisation (Emerson, W. 1962).

Particles were produced using CuO as the active phase and bentonite as the supporting phase. These particles have been produced according to Table 7.1

Table 7.1 Particles produced using CuO with Bentonite as the supporting phase.

Sample Designation	Wt% CuO	Wt% Bentonite
CuO90B10	90	10
CuO80B20	80	20
CuO60B40	60	40

7.3 Particle Characterisation

Characterisation testing has been carried out on samples of these particles. Table 7.2 shows the average crushing strength taken from 30 particles, apparent density and bulk density of the particles. Bulk density was measured by pouring a small sample (a few ml) of particles into a measuring cylinder, tapping the cylinder 5 times to settle the particles, and recording the exact volume that the particles filled. The sample were then weighed. This data were then used to determine bulk density by Eq 7.1 where m = mass of sample, v = volume of sample, and d = bulk density.

$m / v = d$ Eq 7.1

However, this method does not account for the volume of air between the particles. In order to determine the true density of the particles, water was added to a measuring cylinder and the volume recorded. A sample of particles was then weighed, and poured into the water. The new volume of water and particles was measured. This method enabled the exact volume of the particles to be measured. Eq 7.1 was then used with this new value of volume to determine true density.

Table 7.2 Average crushing strength, bulk density and true density of produced particles

Sample	Crushing Strength (N)	Bulk Density (g/ml)	True Density (g/ml)
CuO90B10	1.1	1.9	5.2
CuO80B20	1.6	1.8	4.5
CuO60B40	2.2	1.5	4.2

Table 7.3 shows the oxygen available per unit mass of oxygen carrier for both the CuO/Cu and CuO/Cu_2O systems.

Table 7.3 Oxygen carrying capacity of produced oxygen carriers.

Sample	Oxygen carrying capacity CuO/Cu (kgO_2/kgOC)	Oxygen carrying capacity CuO/Cu_2O (kgO_2/kgOC)
CuO90B10	0.18	0.09
CuO80B20	0.16	0.08
CuO60B40	0.12	0.06

Characterisation of the freshly produced particles was carried out using a number of methods. High magnification of between 5000x, and 20000x SEM-FEG imaging was carried out. Particles of sample were stuck to adhesive carbon tape and mounted in the SEM imager. The lower magnification images indicated the morphology of the particles. The higher magnification images showed the presence or absence of sintering in the particles.

XRD characterisation was performed to determine the species present in the particles. This was used to find the presence of copper II oxide and any copper I oxide that may be present. It was also used to detect any species formed by reaction of copper oxide and bentonite. The samples were crushed to a powder, packed into a sample slide, and mounted in the X ray diffractometer. The device used was a Bruker D8 X ray diffractometer. XRD was carried out in the range of 2θ between 10 – 90^{o}.

Crushing strength tests were performed on the particles. This is intended to be used as a rough guide to how well the particles will withstand attrition in a full size rig. It is expected that particles must have better than 1 N crushing strength in order be used in a full size rig. The results will also serve as a comparison with particles produced on other studies. This was carried out using a Shimpo force gauge. 30 tests were performed on each sample and took the average crushing strength and range of crushing strength from each sample.

7.4 Thermogravimetric Analysis

In order to test the performance of the particles with fuel, 10 cycles were carried out with the particles in a TGA. Each sample was subjected to 10 cycles of oxidation and reduction. The oxidation cycles were carried out in air diluted with nitrogen to 5% oxygen. This concentration of oxygen is used, as it is the concentration of oxygen usually found at the outlet of an air reactor in a CLC plant. The reduction cycles were carried out in 10% CO. A 2 minute purge period occurred between oxidation and reduction. Total flow rate of gas was 200 ml/min. The period of the reduction cycle was 4 minutes, which easily achieved full reduction. It was found that oxidation from Cu2O to CuO occurred slowly, with the particles unable to reach full oxidation. This is discussed further in a later section, but due to this, the period of the oxidation cycle was 20 mins. The sample

size used was 10 mg +/-3 mg. The conditions used here are summarised in Table 7.4 below.

7.5 Fluid Bed Reactor Testing

A small fluid bed reactor was used to test the oxygen release characteristics of the 3 types of particle over a range of temperatures. The samples were tested at 880ºC, 900ºC, 920ºC, and 940ºC. The samples would undergo 10 cycles of oxidation and reduction. The oxidation phase would be in 95% N_2 and 5% O_2, while the reduction phase would be in 100% N_2. Again, this concentration of oxygen is used, as it is the concentration of oxygen usually found at the outlet of an air reactor in a CLC plant. 2.85 L of N_2 was used in both the oxidation and reduction phase and 0.15 L of O_2 in the oxidation phase. The samples were loaded into a quartz reaction tube, which was lowered into the furnace. The samples were heated up to temperature under N_2 flow, then, when at temperature, the cycles were started. Each oxidation and reduction phase lasted 6 minutes. Attrition was measured after the cycles by weighing the filter. The conditions used are summarised in Table 7.4

Table 7.4 Conditions used for testing particles in fluidised bed and TGA.

Particles Tested	Sample Size	Temperatures Tested	Purge Period Duration	Oxidation Duration	Reduction Duration
Fluidised Bed	60 g	880ºC, 900ºC, 920ºC, 940ºC	N/A	6 minutes	6 minutes
TGA	10 mg +/- 3mg	880ºC, 900ºC, 920ºC, 940ºC	2 minutes	20 minutes	4 minutes

The temperature range of 880ºC to 940ºC was selected, because this is the range of temperatures relevant to CLOU behaviour for copper oxides. Around 880ºC, there should be little CLOU activity. Around 940ºC, the equilibrium concentration

of oxygen at the surface of copper oxide is approximately 5%, meaning that oxidation of the particles would not be possible in these tests. This is discussed in detail in a later section. The duration of cycles in the fluid bed test was selected to provide reasonable time for oxidation and reduction of the particles. In prior studies, such as Adanez-Rubio et al., (Adánez-Rubio et al., 2012), and Gayan et al., (Gayán et al., 2012) show that these cycles should take approximately 1 minute each. These cycle times were selected to give ample time for reaction while accounting for additional time required for adverse effects. In the TGA testing, it was found that the oxidation reaction required significantly longer to complete, therefore the longer reaction time of 20 minutes was used.

7.6 Fluidisation of Particles

In order to carry out the fluid bed tests, it was necessary to calculate to volume of gas to supply to achieve fluidisation of the oxygen carrier particles. Fluidisation occurs when the upward drag force exerted by a flowing gas equals to weight of a particle. For a particular particle, at a given temperature in a given gas, the drag force exerted by the gas can be controlled by the velocity of the gas. The velocity of the gas at the point where drag force is equal to the weight of the particle is known as minimum fluidisation velocity, which is denoted as u_{mf}. Minimum fluidisation velocity can be given by Eq 7.2

$$\frac{1.75}{{\varepsilon_{mf}}^3 \varphi_s}.\left(\frac{d_p u_{mf} \rho_g}{\mu}\right)^2 + \frac{150(1-u_{mf})}{{\varepsilon_{mf}}^3 {\varphi_s}^2}.\left(\frac{d_p u_{mf} \rho_g}{\mu}\right) = \frac{{d_p}^3 \rho_g (\rho_s - \rho_g) g}{\mu^2} \quad \text{Eq 7.2}$$

This can be simplified to Eq 7.3 where the Reynolds number <20 (Kunii and Levenspiel, 1991)

$$u_{mf} = \frac{{d_p}^2 (\rho_s - \rho_g) g}{150\mu}.\frac{{\varepsilon_{mf}}^3 {\varphi_s}^2}{1-\varepsilon_{mf}} \quad \text{Eq 7.3}$$

In these equations, u_{mf} = minimum fluidisation velocity, d_p = particle diameter, ρ_s = solid density, ρ_g = gas density, μ = gas dynamic viscosity, ε_{mf} = voidage at minimum fluidisation, φ_s = sphericity and g = gravity.

Reynolds number is the ratio of inertial forces to viscous forces. In this system, the definition of Reynolds number, Re can be given by Eq 7.4

$$Re = \frac{d_p u_{mf} \rho_g}{\mu} \qquad \text{Eq 7.4}$$

This requires that we already know the minimum fluidisation velocity. For particles of the type used in this study, the study headed by Chichester (Chichester et al., 1984) recommends Eq 7.5 to determine Re if minimum fluidisation velocity has not been determined.

$$Re = [(28.7)^2 + 0.0494\,.Ar]^{0.5} - 28.7 \qquad \text{Eq 7.5}$$

Here, Ar =Archimedes number. Archimedes number is a quality used to describe particles in fluid and is the ratio of buoyancy to inertial forces. In this system it is defined by Eq 7.6

$$Ar = {d_p}^3 \rho_g (\rho_s - \rho_g) g / \mu^2 \qquad \text{Eq 7.6}$$

These terms can all be measured for the particles that have been produced, or are known values. As noted in the particle production section above, the solid density figures for the Cu60B40, Cu80B20 and Cu90B10 particles are 4.2 g/ml, 4.5 g/ml and 5.2 g/ml respectively. The particle diameter ranges from 250-500 μm. From sieving the particles to size, it was found that the vast majority of particles were in the 250-350 μm size range. For this reason the particle diameter used is 300 μm. The Archimedes number and Reynolds number depend on the gas density and viscosity, which themselves are dependent on temperature. This results in a range of Archimedes and Reynolds numbers across the 4 temperatures used in this study for each particle type. The gas density and viscosity values used will be those of nitrogen, as the fluidising gas will be either 100% N_2, or 95% N_2. At 880°C, the density of N_2 is 0.29 kg/m^3 and the viscosity is 45.6x10^{-6} Pa.s. at 900°C, the density is 0.287 kg/m^3 and the viscosity is

$46.19x10^{-6}$ Pa.s. At 920ºC, the density is 0.28 kg/m^3 and the viscosity is $46.7x10^{-6}$ Pa.s. At 940ºC, the density is 0.27 kg/m^3 and the viscosity is $47.2x10^{-6}$ Pa.s. The Archimedes numbers for Cu60B40 range from 134.7 at 940ºC to 155 at 880ºC. For the Cu80B20 particles, Archimedes number ranges from 144.3 at 940ºC, to 166 at 880ºC. For the Cu90B10 particles, Archimedes number ranges from 166.7 at 940ºC, to 191.9 at 880ºC. Having the Archimedes number now allows us to use eq 7.4 to determine Reynolds numbers for these systems. For Cu60B40 particles, Reynolds number varies from 0.11 at 940ºC, to 0.13 at 880ºC. For Cu80B20 particles, Reynolds number ranges from 0.12 at 940ºC to 0.14 t 880ºC. For Cu90B10 particles, Reynolds number varies from 0.14 at 940ºC, to 0.16 at 880ºC.

The sphericity of these particles is not high, due to the crushing section of the production procedure. This leads to morphology close to that of crushed glass, sharp sand or pulverised coal. The values of sphericity are taken from (Kunii and Levenspiel, 1991). The figure used for sphericity is 0.6. During the density measurement testing, the void fraction of the freshly settled particles was also determined. The voidage for the Cu60B40, Cu80B20 and Cu90B10 particles was found to be 0.64, 0.6 and 0.63 respectively. The figures for minimum fluidisation velocity calculated for each particle type and temperature are given in Table 7.5

Table 7.5 Minimum fluidisation velocities for each particle type at each temperature used.

	Cu60B40	Cu80B20	Cu90B10
880ºC	0.122 m/s	0.131 m/s	0.151 m/s
900ºC	0.12 m/s	0.129 m/s	0.149 m/s
920ºC	0.119 m/s	0.128 m/s	0.147 m/s
940ºC	0.118 m/s	0.126 m/s	0.146 m/s

The minimum fluidisation velocity must be used to determine a volume flow for minimum fluidisation in order to be used to give a minimum gas flow rate

applicable to these tests. This is a simple process given by Eq 7.7, using radius of the reaction vessel, which in this case is 0.016 m. Therefore the cross-sectional area of the vessel is 0.0008 m^2.

$$V_{mf} = \mu_{mf} A_v \qquad \text{Eq 7.7}$$

Here V_{mf} = volume flow rate at minimum fluidisation, and A_v = cross-sectional area of the reaction vessel. This figure must then be converted to give a corresponding volume flow rate at room temperature given by the mass flow controller to give the volumetric flow rate once the gas has been heated to the temperature of the reaction vessel. This is given by Eq 7.8.

$$V_{fc} = \left(V_{mf}.273\right)/(273 + T) \qquad \text{Eq 7.8}$$

Here T = temperature. This gives the minimum required volumetric flow rate to be used in these tests. This was multiplied by 2 to ensure good fluidisation. For the range of particles and temperatures used in this testing, this gave values around 3 l/m, which is the volumetric flow rate of fluidising gas that were used in these tests.

8 Results

8.1 Thermogravimetric Analysis

When interpreting these results, it is useful it convert the weight change of the sample to conversion, or X. In oxidation, conversion is given by Eq 8.1. In reduction, conversion is given by Eq 8.2.

$$X_{ox} = \frac{m - m_r}{m_o - m_r} \qquad \text{Eq 8.1}$$

$$X_{red} = \frac{m_o - m}{m_o - m_r} \qquad \text{Eq 8.2}$$

Where X = conversion, m = actual mass of sample, m_o = mass of the sample when fully oxidised, and m_r = mass of the sample when fully reduced. The appendix contains graphs showing maximum oxidation conversion as a function of cycle number.

Cu90B10 particles tested at 940ºC weighed 16.9 mg. The expected loss of mass due to reduction to Cu_2O is 1.53 mg, and the expected loss due to reduction to Cu is 3.06 mg. The particles always achieved full reduction with CO, but were not able to achieve full oxidation. Table 8.1a shows full oxidation achieved at each temperature. These start at cycle 2, as cycle 1 was carried out before reduction had occurred, and conversion was full X=1. The final column shows conversion as a function of cycle number for that temperature. Table 8.1b shows the rates of oxidation of Cu90B10 particles at cycle 2, 5 and 10. Table 8.1c shows those rates for reduction. Some of the oxidation cycles show complex behaviour, with 2 distinct phases of oxidation with 2 different rates. Where this is the case, both rates are shown. The units of rate here are mgO_2/mgOC.s, which is mg of oxygen per mg of oxygen carrier per second.

Table 8.1a Oxidation Conversion of Cu90B10 Particles in TGA Testing.

Temp	Cycle 2	Cycle 4	Cycle 6	Cycle 8	Cycle 10	Y=fx
940ºC	0.63	0.54	0.53	0.52	0.52	$Y=0.64X^{-0.1}$
920ºC	0.73	0.65	0.64	0.64	0.64	$Y=0.74x^{-0.07}$
900ºC	0.83	0.77	0.77	0.77	0.78	$Y=0.82x^{-0.03}$
880ºC	0.75	0.69	0.69	0.7	0.7	$Y=0.74x^{-0.03}$

Table 8.1b Oxidation Rate of Cu90B10 Particles in TGA Testing.

Cycle no	940ºC	920ºC	900ºC	880ºC
2	$1.3x10^{-3}$	$1.5x10^{-3}$	$1.9x10^{-3}$	$1.2x10^{-3}$, $6.8x10^{-5}$
5	$5x10^{-4}$	$1x10^{-3}$, $1.3x10^{-4}$	$1.5x10^{-3}$, $1.2x10^{-4}$	$7.6x10^{-4}$, $5.7x10^{-5}$
10	$3.3x10^{-4}$	$6x10^{-4}$, $1x10^{-4}$	$1.2x10^{-3}$, $1.3x10^{-4}$	$1.25x10^{-3}$, $1.7x10^{-4}$

Table 8.1c Reduction Rate of Cu90B10 Particles in TGA Testing.

Cycle no	940ºC	920ºC	900ºC	880ºC
2	$9.2x10^{-4}$	$1x10^{-3}$	$1.55x10^{-3}$	$1.0x10^{-3}$
5	$7.9x10^{-4}$	$7.7x10^{-4}$	$1.55x10^{-3}$	$9.1x10^{-4}$
10	$7x10^{-4}$	$7.7x10^{-4}$	$1.55x10^{-3}$	$9.1x10^{-4}$

As can be seen from Table 8.1a, on cycle 2, the maximum X_{ox} varies from X_{ox}=0.63 at 940ºC, to X_{ox}=0.83 at 900ºC. In addition, maximum X_{ox} will always decrease with increasing cycles. Particularly noteworthy is the maximum X_{ox} at 940ºC, from cycle 4 onwards. This is very close to X_{ox}=0.5, which indicates that the particles are not able to oxidise past Cu_2O. This is supported by the fact that the oxidation rate has only 1 stage, as shown in table 8.1b.

The rates shown are averages over for that cycle. The complex behaviour of oxidation for these particles is interesting. The particles show several stages of oxidation. These different stages correspond to oxidation to different oxides of copper. The fastest oxidation rate corresponds to oxidation to Cu_2O. From there, oxidation slows down and corresponds to oxidation to CuO. The driving forces for these reactions are different, and the oxidation from Cu_2O to CuO is relevant to CLOU investigation. The driving force for this, slower reaction is discussed in the Discussion section. The particles also show an extremely slow final stage of oxidation. X_{ox} achieved in this stage is less than X_{ox}=0.1 and continues to the end of the 20 minute oxidation phase. The rate in this stage is very low, close to

$1.3x10^{-5}$ mgO_2/mgOC.s. This rate is so slow, that it is not possible to take advantage of in an industrial setting, and oxidation is considered to have effectively ended in this stage. For this reason, this stage will not be commented upon further. The rates of oxidation in some cases are actually defined very well by a curve of equation shown below in Eq 8.3.

$$y = a.ln(x) - b \qquad \text{Eq 8.3}$$

Where a and b are numbers lower than 1 with a value around 0.15. These have been presented in the form in the table to allow comparison to the other rates. Cycles 5, 10 at 920ºC, and cycle 10 at 900ºC show this behaviour. This behaviour is shown by particles which can oxidise to CuO, but where sintering has occurred. This behaviour is likely caused by a shell of reacted material forming, which restricts further reaction and forces ion diffusion to dominate. Rate modelling is beyond the scope of this thesis, but is discussed in the conclusion section.

The rates in cycle 2 at 940ºC, 920ºC, and 880ºC are roughly similar, at $1.3x10^{-3}$, $1.5x10^{-3}$, and $1.2x10^{-3}$ mgO_2/mgOC.s respectively. At 900ºC the rate is $1.9x10^{-3}$ mgO_2/mgOC.s which is the highest rate. These rates all drop off steadily. Where a second stage of oxidation takes place, this is generally much slower than the first stage, e.g. at 900ºC, where the rate changes from $1.5x10^{-3}$ mgO_2/mgOC.s to $1.2x10^{-4}$ mgO_2/mgOC.s, which less than $1/10^{th}$ the rate of the first stage. Over the 10 cycles at all temperatures, oxidation slows and becomes a steady curve. At 920ºC for this curve dX/dt=0.127/t, at 900ºC dX/dt=0.137/t and at 880ºC dX/dt=0.143/t. In terms of mgO_2/mgOC.s, the rates for these temperatures are 0.35/t mgO_2/mgOC.s, 0.22/t mgO_2/mgOC.s and 0.14/t mgO_2/mgOC.s respectively.

Reduction always reaches X_{red}=1 in all cycles at all temperatures. The reactivity of both CuO and Cu_2O with CO are high, and the kinetics allow full conversion to metallic Cu. As table 8.1c shows, at cycle 2, the rate starts at around $1x10^{-3}$ mgO_2/mgOC.s. The highest rate is again at 900ºC, at $1.55x10^{-3}$ mgO_2/mgOC.s. At this temperature, the rate also remains steady across all cycles. At the other

temperatures, the rate drops slightly, with the lowest rate being at 940ºC. however, the loss in performance is not as severe as the loss in oxidation performance.

For the particles designated Cu80B20, Tables 8.2a, b, and c show maximum oxidation conversion, oxidation and reduction rates, respectively, across all temperatures.

Table 8.2a Oxidation Conversion of Cu80B20 Particles in TGA Testing.

Temp	Cycle 2	Cycle 4	Cycle 6	Cycle 8	Cycle 10	Y=fx
940ºC	0.64	0.54	0.53	0.52	0.52	$Y=0.65x^{-0.1}$
920ºC	0.83	0.77	0.75	0.74	0.72	$Y=0.87x^{-0.08}$
900ºC	0.76	0.73	0.72	0.71	0.71	$Y=0.78x^{-0.04}$
880ºC	0.78	0.77	0.76	0.77	0.78	Y=0.77

Table 8.2b Oxidation Rate of Cu80B20 Particles in TGA Testing.

Cycle no	940ºC	920ºC	900ºC	880ºC
2	$1x10^{-3}$, $1.2x10^{-5}$	$2.2x10^{-3}$, $2x10^{-4}$	$8.9x10^{-4}$	$1.6x10^{-3}$
5	$4.4x10^{-4}$	$1.3x10^{-3}$, $1x10^{-4}$	$5.9x10^{-4}$	$9.7x10^{-4}$, $3.5x10^{-5}$
10	$4.4x10^{-4}$	$1x10^{-3}$, $7.8x10^{-5}$	$6.2x10^{-4}$, $2.9x10^{-4}$	$1x10^{-3}$, $8x10^{-5}$

Table 8.2c Reduction Rate of Cu80B20 Particles in TGA Testing.

Cycle no	940ºC	920ºC	900ºC	880ºC
2	$1.2x10^{-3}$	$1.5x10^{-3}$	$1.2x10^{-3}$	$1.2x10^{-3}$
5	$8.4x10^{-4}$	$1.3x10^{-4}$	$9x10^{-4}$	$1x10^{-3}$
10	$8.4x10^{-4}$	$8.6x10^{-4}$	$9x10^{-4}$	$1x10^{-3}$

The maximum oxidation conversion for Cu80B20 particles decreases over progressive cycles as with Cu90B10 particles, as shown in Table 8.2a. This is true for temperatures except for 880°C, where maximum conversion remains approximately X_{ox}=0.77 during all cycles. This is an interesting feature which will be considered in the Discussion section. Reduction conversion during the purge phase is lowest at 880°C, as expected, at approximately X_{red}=0.1. This is highest at 920°C, where X_{red}=0.22. During reduction in CO, X_{red}=1 in all cases.

Table 8.2b shows that at 940°C, in cycle 2 there are 2 oxidation stages at the second stage is the oxidation from X_{ox}=0.5 to X_{ox}=0.64 and is very slow. The cycles after this only have 1 stage of oxidation. Table 8.2a also shows that these particles are unable to oxidise past X_{ox}=0.5 after cycle 4. This indicates that at this temperature, the particles lose the ability to oxidise from Cu_2O to CuO. At 900°C, only 1 stage of oxidation is shown in cycles 2 and 5. In these cycles, there are very fast rates, $8.9x10^{-4}$ mgO_2/mgOC.s and $5.9x10^{-4}$ mgO_2/mgOC.s respectively, where the particles oxidise to approx. X_{ox}=0.65. The remaining conversion takes place very slowly over the following 18 minutes of the oxidation cycle. By the 10th cycle, this performance has been lost and the particles only reach X_{ox}=0.4 in the fast oxidation stage. Performance is lost in progressive cycles at all temperatures. At 920°C, the first stage of oxidation is fast, but only reaches X_{ox}=0.5, and the rate slows significantly after this. At the other temperatures, the particles oxidise to approximately X_{ox}=0.65, as mentioned above. As Table 8.2c shows, the Cu80B20 particles show lowering of rate of reduction as cycles increase across all temperatures. This is similar to the behaviour of the Cu90B10 particles. The highest rate is $1.5x10^{-3}$ mgO_2/mgOC.s at 920°C, although, as mentioned, the rate drops, and at the 5th cycle, the rate is $1.3x10^{-4}$ mgO_2/mgOC.s. This has fallen again to $8.6x10^{-4}$ mgO_2/mgOC.s at the 10th cycle.

Tables 8.3a, b, and c show maximum oxidation conversion, oxidation and reduction rates, respectively, across all temperatures for the CU60B40 particles.

Table 8.3a Oxidation Conversion of Cu60B40 Particles in TGA Testing.

Temp	Cycle 2	Cycle 4	Cycle 6	Cycle 8	Cycle 10	Y=fx
940ºC	0.64	0.54	0.52	0.52	0.52	$Y=0.63x^{-0.09}$
920ºC	0.82	0.79	0.80	0.80	0.80	Y=0.8
900ºC	0.84	0.84	0.84	0.84	0.83	Y=0.84
880ºC	0.83	0.83	0.82	0.83	0.83	Y=0.83

Table 8.3b Oxidation Rate of Cu60B40 Particles in TGA Testing.

Cycle no	940ºC	920ºC	900ºC	880ºC
2	$1.6x10^{-3}$, $2.3x10^{-5}$	$1.4x10^{-3}$, $1.7x10^{-4}$	$7x10^{-4}$, $1.1x10^{-5}$	$8.8x10^{-4}$, $2.1x10^{-5}$
5	$8.5x10^{-4}$	$1x10^{-3}$, $1x10^{-4}$	$5.7x10^{-4}$, $1.1x10^{-5}$	$8.8x10^{-4}$, $2.1x10^{-5}$
10	$3.0x10^{-4}$	$1x10^{-3}$, $1x10^{-4}$	$5.7x10^{-4}$, $1.1x10^{-5}$	$8.8x10^{-4}$, $2.1x10^{-5}$

Table 8.3c Reduction Rate of Cu60B40 Particles in TGA Testing.

Cycle no	940ºC	920ºC	900ºC	880ºC
2	$1.0x10^{-3}$	$1.0x10^{-3}$	$1.2x10^{-3}$	$1.0x10^{-3}$
5	$1.0x10^{-3}$	$6.9x10^{-4}$	$9.0x10^{-4}$	$1.0x10^{-3}$
10	$1.0x10^{-3}$	$6.9x10^{-4}$	$9.0x10^{-4}$	$1.0x10^{-3}$

The X_{ox} conversion statistics shown in Table 8.3a indicate that the Cu60B40 particles are able to reach very close to the same X_{ox} across all 10 cycles at 920ºC, 900ºC, and 880ºC. This is not the case at 940ºC, where the conversion varies by $0.63x^{-0.09}$ as a function of cycle number, where x is cycle number. At this temperature, conversion is unable to progress past X_{ox}= 0.54 by the 4^{th} cycle. This information can be investigated with information from Table 8.3b, which shows that the particles only have 1 stage of oxidation. This indicates that the particles are unable to oxidise past Cu_2O, as with the other particle types.

However, at the other 3 temperatures, the particles are able to reach a high level of conversion, and to maintain their performance across all 10 cycles. The highest conversion is at 900ºc, where conversion reaches X_{ox}=0.84.

The oxidation rates shown in Table 8.3b do not show figures as high as for the Cu80B20 particles. For instance the highest rate shown by Cu80B20 is $2.2x10^{-3}$ mgO_2/mgOC.s, where as for the CU60B40 particles, it is $1.6x10^{-3}$ mgO_2/mgOC.s. However, these statistics do not take account of how high X_{ox} is able to reach at this rate. For the Cu60B40 particles tested at 900ºC, and 880ºC, the initial stage of oxidation in the second cycle has rates of $7x10^{-4}$ mgO_2/mgOC.s and $8.8x10^{-4}$ mgO_2/mgOC.s respectively. However, these particles are able to reach high conversion at these rates, these conversion values are X_{ox}=0.7 and X_{ox}=0.67 at 900ºC and 880ºC respectively. This means that the Cu60B40 particles are able to achieve higher oxidation conversion at these lower temperatures, than the other particles are. The rate does then slow down however, and the particles achieve an additional X_{ox}=0.14 conversion in the remaining 19 minutes of the oxidation phase. This is still higher than the conversion that the other particles are able to achieve, as shown above.

Table 8.3c shows that at 940ºC, 900ºC, and at 880ºC, the Cu60B40 particles are able to maintain reduction rates very close to $1.0x10^{-3}$ mgO_2/mgOC.s across all 10 cycles. At 900ºC, and 880ºC, all 3 particle types are able to maintain rates of reduction fairly well, as shown in the tables above. Reduction with CO happens quickly and reliably with all particle types. However, the Cu60B40 particles show the ability to achieve X_{red}=0.2 in the nitrogen purge phase at 920ºC, 900ºC, and 880ºC. This behaviour is also shown in the 10^{th} cycle, meaning that the performance is not lost. This is very encouraging for the Cu60B40 particles. The other particles do not show this behaviour in cycle 10, meaning that their CLOU behaviour is affected badly by progressive cycles.

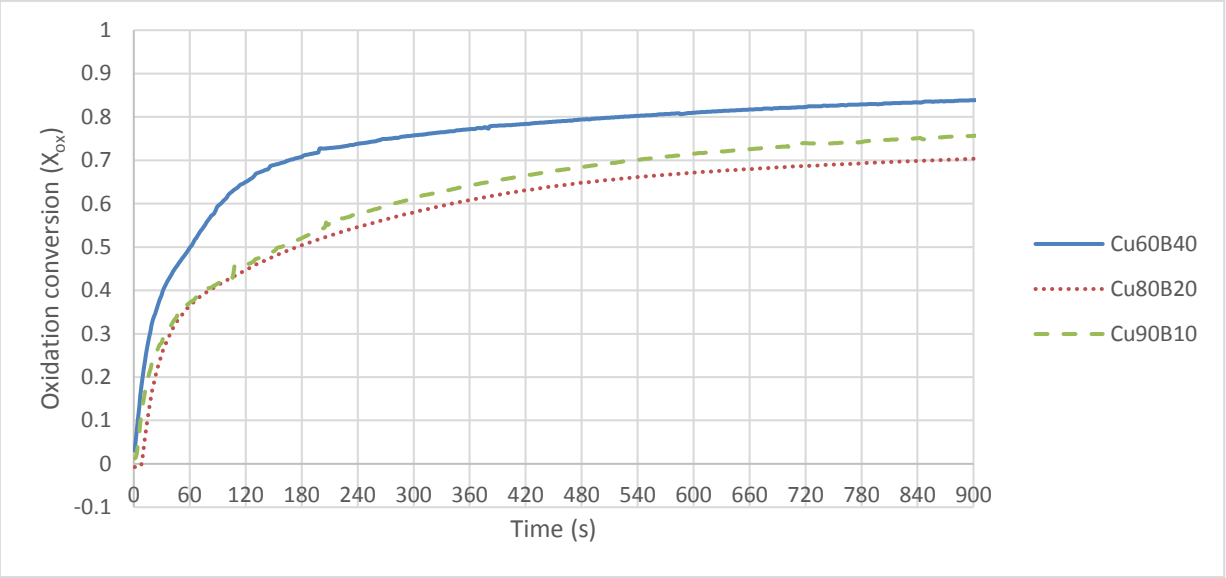

Figure 8.1 Optimum oxidation performance for the 3 particle types at cycle 10.

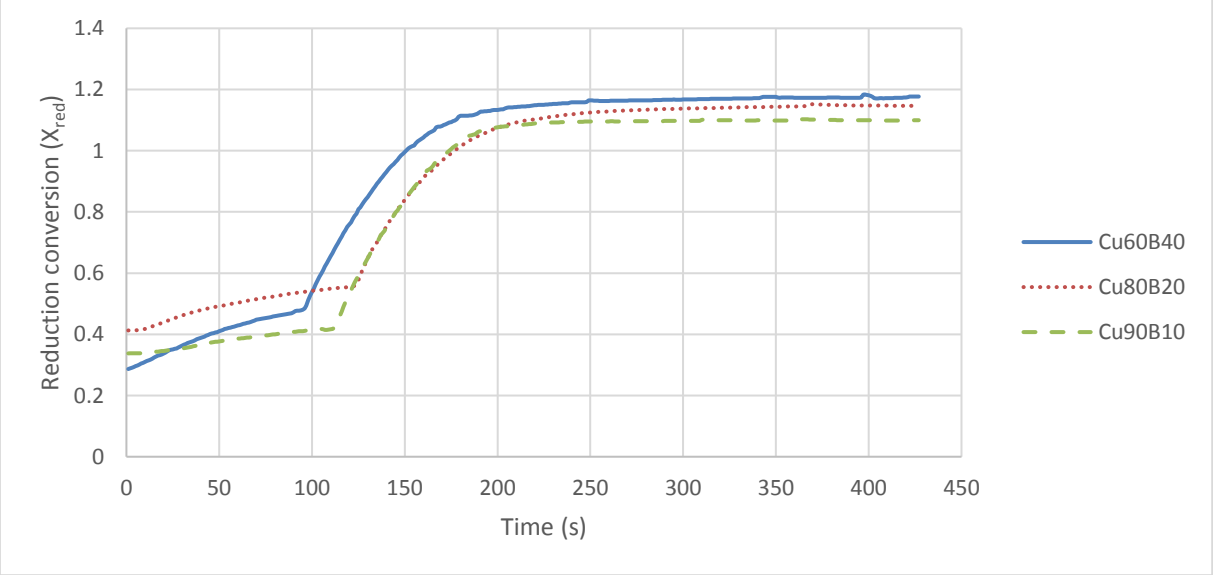

Figure 8.2 Optimum reduction performance for the 3 particle types at cycle 10.

Figure 8.1 shows the change of conversion against time for oxidation cycle 10 of the 3 particle types in their best performing conditions. Figure 8.2 shows the change of conversion against time for reduction cycle 10 of the 3 particle types in their best performing conditions. For Cu90B10 the optimum temperature is 900ºC and for Cu80B20 this is 920ºC. These are the temperatures at which both

oxidation and reduction show the combination of highest X_{ox}, and highest rates of oxidation and reduction. For Cu60B40 the optimum temperature is 900^{o}C. The first stage of reduction, with little change in X_{red} is the purge phase. The performance is fairly similar to 880^{o}C, however the particles are able to reach X_{red}=0.5 in the purge phase at 900^{o}C, and only X_{red}=0.4 at 880^{o}C.

8.2 Fluid Bed testing

The fluid bed tests were carried out in a 32 mm fluidised bed. All testing was carried out at atmospheric pressure. They were used to find the oxygen release characteristics of the particles. The particles were subjected to an N_2 environment at temperatures of 880^{o}C, 900^{o}C, 920^{o}C, and 940^{o}C to investigate the reduction to Cu_2O. They were then oxidised in 5%O_2 in a balance of N_2 and 10 consecutive cycles were carried out at each temperature. The fluid bed testing for the particles designated Cu90B10 was initially carried out at 880^{o}C and 900^{o}C. After both these tests, there was a large pressure drop recorded across the bed. After the samples were removed from the reaction tube, they were found to have clumped together. The clumping indicates that the particles defluidised during the testing. It was determined that the defluidisation occurred when the pressure drop across the bed increased significantly. Due to this, these tests were repeated. For the particles designated Cu90B10, 91 g of oxygen carrier was used. Of this weight, 90% was the CuO active phase. This equates to 81.9 g of CuO. The molecular weight of CuO is 63 + 16 = 79. Therefore there are 81.9/79 = 1.04 mols of CuO. When the oxygen carrier has reached theoretical full conversion in the reduction phase it will have the formula Cu_2O. The oxygen carrier will therefore release 0.25 mols of O_2 per mol of CuO at full conversion. The maximum possible mols of O_2 that the oxygen carrier could release in reduction is 0.26 mols. O_2 has a molecular weight of 32, meaning this equates to 8.3 g of O_2. For the Particles designated Cu80B20 in the cycles carried out at 880^{o}C, 70.4 g of oxygen carrier were used. There was 80% by weight of CuO powder used, meaning 56.3 g of CuO. The maximum possible mols of O_2 that could be released is 0.18 when

reduced to Cu_2O. This is 5.7 g of O_2 which can be released. For the cycles carried out at 900ºC, 920ºC, and 940ºC, 72 g of oxygen carrier were used, being 57.6 g of CuO. At full reduction to Cu_2O, 0.18 mols of O_2 can be released, which is 5.8 g. For the particles designated Cu60B40, 62 g of oxygen carrier were used in all cycles. Of this weight, 60% was CuO powder, meaning there is 37.2 g of active CuO phase. At full reduction to Cu_2O, 0.12 mols of O_2 will be released, this is 3.7 g of O_2.

The graphs show partial pressure of oxygen in the y axis and time in seconds on the x axis. In oxidation, the curves increase from 0% to 5% more slowly, with a shallower slope, or more quickly, with a steeper curve, relative to each other. Where a curve is steeper, the oxygen concentration is increasing more quickly, and the oxygen carrier particles are reacting more slowly with the oxygen, with a lower total amount of oxidation. Where a curve is shallower, the oxygen concentration is increasing more slowly, meaning that the oxygen carrier particles are reacting more quickly with more of the available oxygen. This means a higher oxidation rate. In reduction, the curve reduces from 5% to 0%. If the curve is steeper, the oxygen concentration is reducing more quickly. Again this indicates that the particles are releasing oxygen more slowly, with a lower total amount of released oxygen. If the curve is shallower, then the oxygen concentration is reducing more slowly. This indicates that the particles are releasing oxygen more quickly, with a higher total amount of released oxygen.

Table 8.4a Reduction rates achieved for Cu90B10 Particles

Temperature	Cycle 1	Cycle 5	Cycle 10
940	$Y=-3x10^{-5}\ln(x)+0.0001$	$Y=-3x10^{-5}\ln(x)+0.0001$	$Y=-4x10^{-5}\ln(x)+0.0001$
920	$Y=-1x10^{-5}\ln(x)+0.00007$	$Y=-9x10^{-6}\ln(x)+0.00004$	$Y=-3x10^{-6}\ln(x)+0.00002$
900	$Y=-5x10^{-5}\ln(x)+0.00004$	$Y=-3x10^{-5}\ln(x)+0.00003$	$Y=-3x10^{-5}\ln(x)+0.00003$
880	$Y=-3x10^{-5}\ln(x)+0.0001$	$Y=-1x10^{-5}\ln(x)+0.00006$	$Y=-1x10^{-5}\ln(x)+0.00007$

Table 8.4b Oxidation rates achieved for Cu90B10 Particles

Temperature	Cycle 1	Cycle 5	Cycle 10
940	$Y=-5x10^{-5}\ln(x)+0.0002$	$Y=-2x10^{-5}\ln(x)+0.00007$	$Y=-3x10^{-5}\ln(x)+0.0001$
920	$Y=-4x10^{-5}\ln(x)+0.0002$	$Y=-8x10^{-6}\ln(x)+0.00005$	$Y=-5x10^{-6}\ln(x)+0.00004$
900	$Y=-3x10^{-5}\ln(x)+0.0002$	$Y=-2x10^{-5}\ln(x)+0.0001$	$Y=-2x10^{-5}\ln(x)+0.0001$
880	$Y=-3x10^{-5}\ln(x)+0.0001$	$Y=-2x10^{-5}\ln(x)+0.00008$	$Y=-1x10^{-5}\ln(x)+0.00007$

Table 8.4a shows reduction rates for Cu90B10 particles at all temperatures at cycle 1, 5, and 10. Table 8.4b shows oxidation rates for Cu90B10 particles at all temperatures at cycle 1, 5, and 10. The units on the y axis are moles O_2 per second. As tables 8.4a and 8.4b show, the differences between the different temperatures and cycles are very low. For example, in reduction, the fastest rate, which is at 940^{o}C, and is $Y=-3x10^{-5}\ln(x)+0.0001$, and the lowest rate is $Y=-3x10^{-6}\ln(x)+0.00002$. In oxidation, the highest rate is $Y=-3x10^{-5}\ln(x)+0.0002$ at 900^{o}C, in cycle 1. The lowest rate in oxidation is $Y=-8x10^{-6}\ln(x)+0.00005$ at 920^{o}C, in cycle 5. All these rates equate to a very low amount of O_2 per second, and over the full length of the cycle, they equate to less than 4% of the expected amount of oxygen released. Roughly speaking, there is a lowering of rates as cycles increase, as shown by table 8.4a, and table 8.4b.

Table 8.4c Reduction rates achieved for Cu80B20 Particles

Temperature	Cycle 1	Cycle 5	Cycle 10
940	$Y=-5x10^{-6}\ln(x)+0.00003$	$Y=-9x10^{-6}\ln(x)+0.00005$	$Y=-9x10^{-6}\ln(x)+0.00005$
920	$Y=-4x10^{-5}\ln(x)+0.0002$	$Y=-6x10^{-5}\ln(x)+0.0002$	$Y=-4x10^{-6}\ln(x)+0.0002$
900	$Y=-4x10^{-5}\ln(x)+0.0001$	$Y=-6x10^{-5}\ln(x)+0.0001$	$Y=-6x10^{-5}\ln(x)+0.0001$
880	$Y=-4x10^{-5}\ln(x)+0.0002$	$Y=-4x10^{-5}\ln(x)+0.0002$	$Y=-9x10^{-6}\ln(x)+0.00004$

Table 8.4d Oxidation rates achieved for Cu80B20 Particles

Temperature	Cycle 1	Cycle 5	Cycle 10
940	$Y=-3x10^{-5}\ln(x)+0.0001$	$Y=-2x10^{-5}\ln(x)+0.00008$	$Y=-2x10^{-5}\ln(x)+0.00008$
920	$Y=-5x10^{-5}\ln(x)+0.0002$	$Y=-1x10^{-5}\ln(x)+0.00007$	$Y=-4x10^{-5}\ln(x)+0.0002$
900	$Y=-2x10^{-5}\ln(x)+0.00008$	$Y=-1x10^{-5}\ln(x)+0.00007$	$Y=-1x10^{-5}\ln(x)+0.00008$
880	$Y=-1x10^{-5}\ln(x)+0.00007$	$Y=-1x10^{-6}\ln(x)+0.00002$	$Y=-1x10^{-5}\ln(x)+0.00007$

This section will cover the particles designated Cu80B20. Table 8.4c shows reduction rates for Cu80B20 particles at all temperatures at cyle1, 5, and 10. Table 8.4d shows oxidation rates for Cu80B20 particles at all temperatures at cyle1, 5, and 10. After the 10 cycles at 880^{o}C there was an indication of defluidisation. This was shown by a large drop in pressure across the bed, and the sample was found to have clumped up upon inspection. For these particles, again there is little distinction between the temperatures and cycle number. The highest rate shown in reduction is $Y=-4x10^{-5}\ln(x)+0.0002$ at 920^{o}C in cycle 1. The lowest rate is $Y=-9x10^{-6}\ln(x)+0.00004$ at 880^{o}C in cycle 10. In oxidation, the highest rate is $Y=-5x10^{-5}\ln(x)+0.0002$ at 920^{o}C, in cycle 1. The lowest rate is $Y=-1x10^{-6}\ln(x)+0.00002$ at 880^{o}C, in cycle 5. Again, the total amount of reacted oxygen is less than 4% of the theroretical maximum. As with the Cu90B10 particles, table 8.4c, and table 8.4d show that there is a general reduction in rates as cycle number increases. However, in some cases cycle 5 has a lower rate than cycle 10. This is likely due to slight fluctuations in how the gas flows through the apparatus.

Table 8.4e Reduction rates achieved for Cu60B40 Particles

Temperature	Cycle 1	Cycle 5	Cycle 10
940	$Y=-6x10^{-6}\ln(x)+0.00005$	$Y=-8x10^{-6}\ln(x)+0.00006$	$Y=-6x10^{-6}\ln(x)+0.00005$
920	$Y=-2x10^{-5}\ln(x)+0.0001$	$Y=-2x10^{-5}\ln(x)+0.0001$	$Y=-2x10^{-5}\ln(x)+0.0001$
900	$Y=-7x10^{-5}\ln(x)+0.0003$	$Y=-4x10^{-5}\ln(x)+0.0002$	$Y=-3x10^{-5}\ln(x)+0.0001$
880	$Y=-2x10^{-5}\ln(x)+0.0001$	$Y=-1x10^{-5}\ln(x)+0.00005$	$Y=-2x10^{-5}\ln(x)+0.0001$

Table 8.4f Oxidation rates achieved for Cu60B40 Particles

Temperature	Cycle 1	Cycle 5	Cycle 10
940	$Y=-4x10^{-5}\ln(x)+0.0002$	$Y=-3x10^{-5}\ln(x)+0.0001$	$Y=-3x10^{-5}\ln(x)+0.0001$
920	$Y=-1x10^{-4}\ln(x)+0.0004$	$Y=-2x10^{-5}\ln(x)+0.0001$	$Y=-2x10^{-5}\ln(x)+0.00009$
900	$Y=-1x10^{-4}\ln(x)+0.0004$	$Y=-2x10^{-5}\ln(x)+0.0001$	$Y=-2x10^{-5}\ln(x)+0.00009$
880	$Y=-8x10^{-5}\ln(x)+0.0003$	$Y=-8x10^{-6}\ln(x)+0.0004$	$Y=-2x10^{-5}\ln(x)+0.00009$

Finally this section will look at the particles designated Cu60B40. Table 8.4e shows reduction rates for Cu60B40 particles at all temperatures at cycle 1, 5, and 10. Table 8.4f shows oxidation rates for Cu60B40 particles at all temperatures at cycle 1, 5, and 10. The highest rate in reduction is $Y=-7x10^{-5}\ln(x)+0.0003$ at 900^{o}C in cycle 1. The lowest rate is $Y=-6x10^{-6}\ln(x)+0.00005$, which is shown at 940^{o}C. The highest rate in oxidation is $Y=-1x10^{-4}\ln(x)+0.0004$, at 900^{o}C, in cycle 1. The lowest rate is $Y=-2x10^{-5}\ln(x)+0.00009$, which is shown at 920^{o}C, 900^{o}C, and 880^{o}C in cycle 10. The trends shown by these particles are the same as the trends shown by the other 2 particle types. Table 8.4e and table 8.4f show that there is a general reduction in rates as cycle number increases.

An additional comparison which can be made is the comparison between the particles at each temperature. In oxidation, each particle type will fully react in approximately 25 seconds. At all temperatures, the Cu60B40 particles take longer than the Cu90B10 and Cu80B20 particles before they stop oxidising. The oxygen reaction rates are also generally higher throughout each cycle. This indicates that the Cu60B40 particles are able to achieve a greater degree of oxidation conversion than the Cu90B10 and Cu80B20 particles. The Cu80B20 particles show slightly higher oxidation conversion than Cu90B10, though this is not significant, and in some cases the degree of oxidation is the same.

In reduction, the particles take roughly 25 seconds at 940^{o}C, and 30 seconds at 880^{o}C, to reach full conversion. Again, the trend across the 3 different particle types, is that the Cu60B40 particles show a slower drop in oxygen concentration than the other 2 particle types. This indicates that the Cu60B40 particles are able to reach greater reduction conversion than the other 2 particles. This different temperature conditions do not have as significant an effect as the change in oxygen carrier composition. The difference between the 1st cycle and 10th cycle is also not as significant as the oxygen carrier composition.

The best performance is from Cu60B40 particles at 900^{o}C in the first cycle. To determine the amount of oxygen released during reduction, and reacted during oxidation, a baseline of oxygen concentration change, conduction with sand in the fluid bed reactor, was subtracted from the oxygen concentration for each cycle. This was then converted into mols of oxygen using the perfect gas equation and plotted against time. For the best performing cycles, that of Cu60B40 at 900^{o}C, the results are shown in figures 8.3a and 8.3b below. The corresponding data for the Cu80B20 and Cu90B10 particles is also shown for reference.

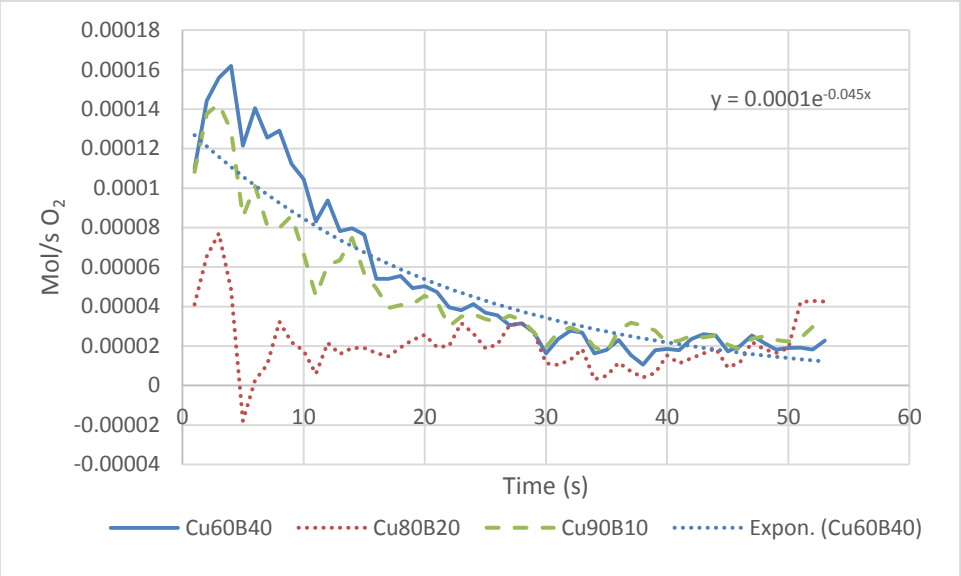

Figure 8.3a Mol of oxygen reacting in oxidation during cycle 5 of particles at 900ºC.

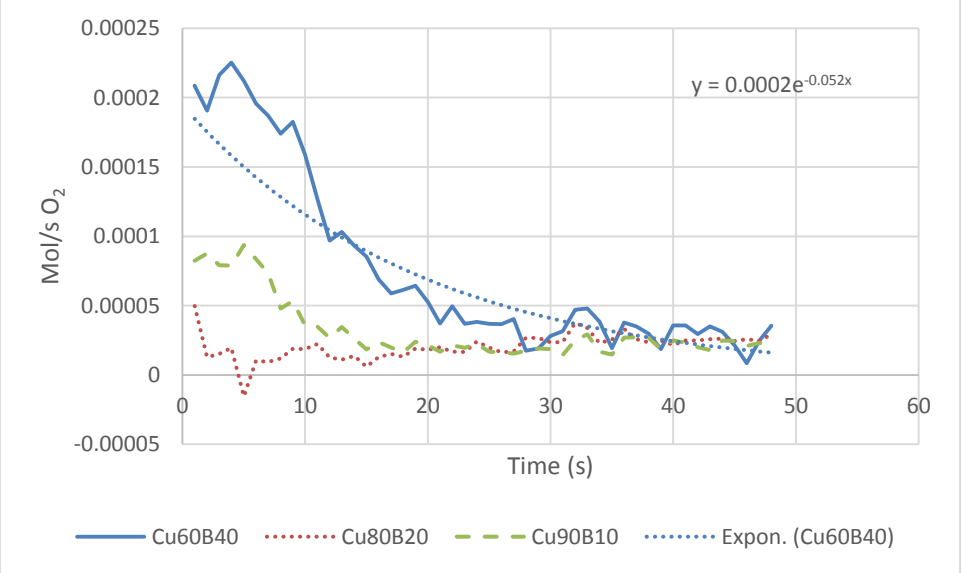

Figure 8.3b Mol of oxygen reacting in reduction during cycle 5 of particles at 900ºC.

Here, 62 g of oxygen carrier was used as the sample. The theoretical maximum amount of O_2 which could react is 0.11 mole. Integration of the curve gives Eq 8.4.

$$\int_0^{360} 0.0002\, e^{(-0.052x)} = \frac{e^{468/25}-1}{260e^{468/25}} = 0.0038\ mole/s \qquad \text{Eq 8.4}$$

The limit of 340 represents the time of reaction in the vessel. This figure is well below the theoretical value. All cycles here achieve around 4% of the theoretical maximum value for conversion. The TGA data show that the particles should be able to reach X=0.4 conversion in ideal conditions, in 2 minutes in an inert atmosphere. Here, the particles are only able to achieve X=0.04 in 6 minutes. The temperatures used for the TGA testing and fluid bed testing were the same, and the atmosphere used was the same, however the flow rate of gas through the sample was very different and may be part of the reason that the difference in conversion was so high. This is discussed further in the Discussion section.

8.3 Characterisation Testing

8.3.1 Crushing Strength Tests

In order to characterise the particles, and to better understand how they changed during reduction and oxidation cycles, characterisation tests were carried out before and after the fluid bed testing. These tests consisted of crushing strength tests, XRD testing, and SEM imaging.

Table 8.5a Average and Standard Deviation Crushing Strength Figures for the 3 Types of Particles Before Fluid Bed Tests.

Pre test	Cu60B40 (N)	Cu80B20 (N)	Cu90B10 (N)
Average	2.3	1.6	1
Standard Deviation	0.7	0.4	0.3

Table 8.5b Average and Standard Deviation Crushing Strength Figures for the 3 Types of Particles After Fluid Bed Tests.

Post test	Cu60B40 (N)	Cu80B20 (N)	Cu90B10 (N)
Average	2.3	2	1.8
Standard Deviation	0.7	0.6	0.7

Crushing strength tests were carried out on 30 of each of the 3 different types of particles after they had been calcined. Table 8.5a shows the average and standard deviation crushing strength figures for the 3 types of particles before fluid bed testing. Table 8.5b shows the same data after fluid bed testing. The tables show that for Cu80B20 and Cu90B10 particles, the average crushing strength actually increases after fluid bed testing. This will be discussed further in the Discussion section.

It is accepted that the lowest crushing strength appropriate for use in an industrial fluid bed is 1 N (Peterson et al., 2013). There are some particles from each type which fall below this threshold. However, the mean, mode and median values of the Cu60B40 and Cu80B20 particles are all higher than 1 N, with the majority of particles having higher than 1 N crushing strength. The Cu90B10 particles have a mean crushing strength value of 1 N, and a mode value of 0.9 N. This indicates that freshly produced Cu90B10 particles are not suitable for use in a large fluid bed. These tests were carried out after calcination at 950^{o}C. Before calcination, the particles had the consistency of wet clay, and were far too soft to carry out crushing strength tests.

The crushing strength tests performed after the fluid bed tests actually show an increase in crushing strength for both the Cu80B20 and Cu90B10 particles. However, the Cu60B40 particles do show a reduction in crushing strength. The Cu60B40 particles after the fluid bed tests do still have mode and median values at 2 N and a mean value above 2 N. There were also found to be no particles

sampled with lower than 1 N crushing strength. When the particle filter from the fluid bed rig was weighed after the fluid bed testing was carried out, there was found to be an extremely small amount of material lost from the bed. It is possible that the softer particles broke into a small number of daughter particles which were still large enough to avoid elutriation.

The CU80B20 and Cu90B10 particles both show an increase in crushing strength. After weighing the fluid bed rig filter following the testing for both of these particles, there was again found to be a very small amount of material elutriated form the bed. It could be argued that the softer particles were destroyed in the fluid bed, as may be expected with particles lower than 1 N. This would mean that only the stronger particles would remain for characterisation after the testing. However this would lead to a large amount of material recovered in the filter, and a significantly reduced amount of material left in the bed when I emptied it. Neither of these two results was found after the fluid bed testing. Considering that the calcination of the particles was carried out close to the temperatures that these particles were tested at in the fluid bed tests, it is reasonable to suggest that the particles experienced further calcination while in the fluid bed tests. This would lead to particles with higher crushing strength and account for the fact that such a small amount of elutriated material was found in the filter. The Cu80B20 particles show mean, mode, and median figures around 2 N, with no particles showing less than 1 N after fluid bed testing. The Cu90B10 particles still had relatively low mean, mode and median figures from crushing strength tests, and showed particles with crushing strength lower than 1 N after fluid bed testing. This indicates that the fluidisation conditions were not as severe in these tests as would be experienced in a full size unit. The fluidisation regime of the particles in these tests was bubbling, not fast fluidised or in riser conditions. However it is reasonable to conclude that the Cu90B10 particles would not be strong enough to stand up to the conditions in a full size riser. However these results indicate that the Cu80B20 and Cu60B40 particles would be able to withstand these conditions with reasonably low elutriation rate.

8.3.2 SFEG Imaging

SFEG imaging was carried out on all three types of particles after they had been calcined, and repeated the imaging after the particles had been through the fluid bed testing. Images of the Cu60B40, Cu80B20, Cu90B10 particles prior to fluid bed testing, and the same after fluid bed testing are shown below in figure 8.5, 8.6, 8.7, 8.8, 8.9, and 8.10 respectively. The images taken of particles freshly calcined show that the particles do not have good sphericity. This is caused by the production process. The images for the 3 different types of particles produced do not show significant differences. The particles are crushed after calcination to remove over-sized particles. The images show distinct areas of smooth, almost featureless areas, and areas of crystalline material. This material appears to have oversized pores running through it. The crystalline areas are CuO. The smooth areas are bentonite holding the CuO particles together. This is illustrated in Figure 8.4.

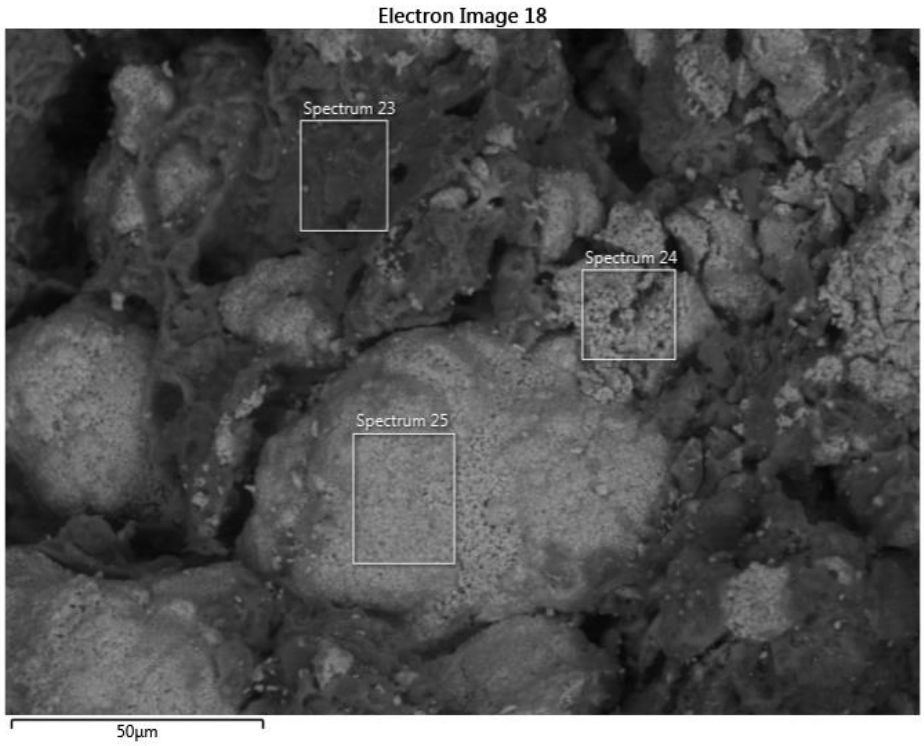

Figure 8.4a SEM image of a Cu60B40 particle with the different areas selected.

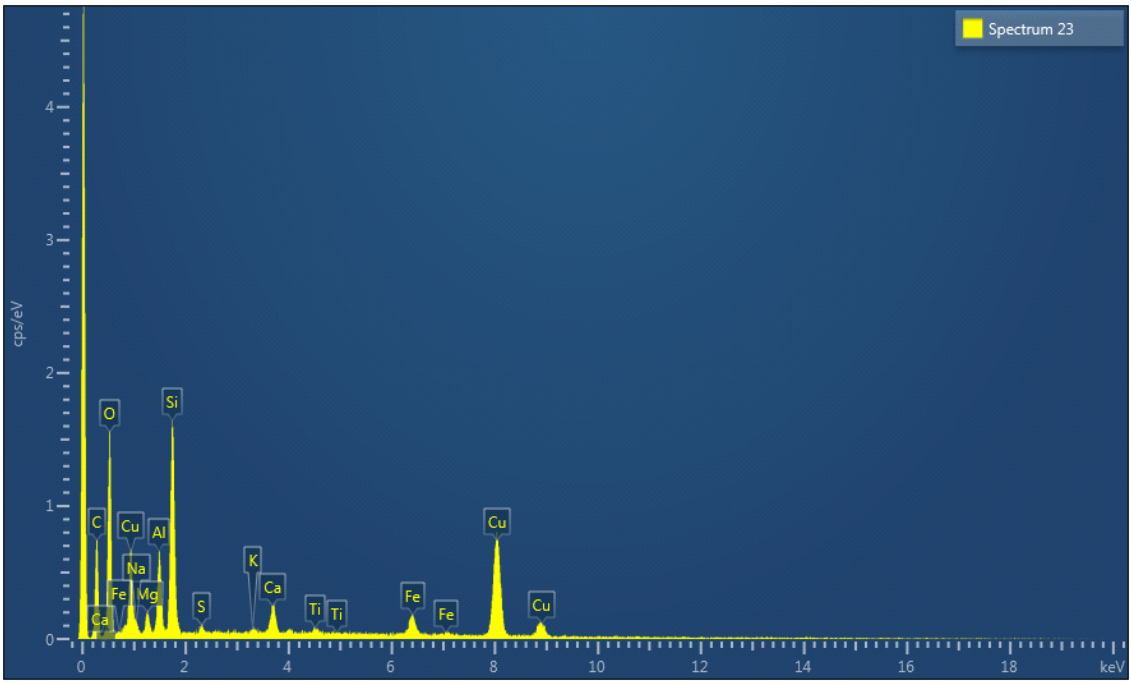

Figure 8.4b Chemical Spectra of area 23 in figure 8.4a.

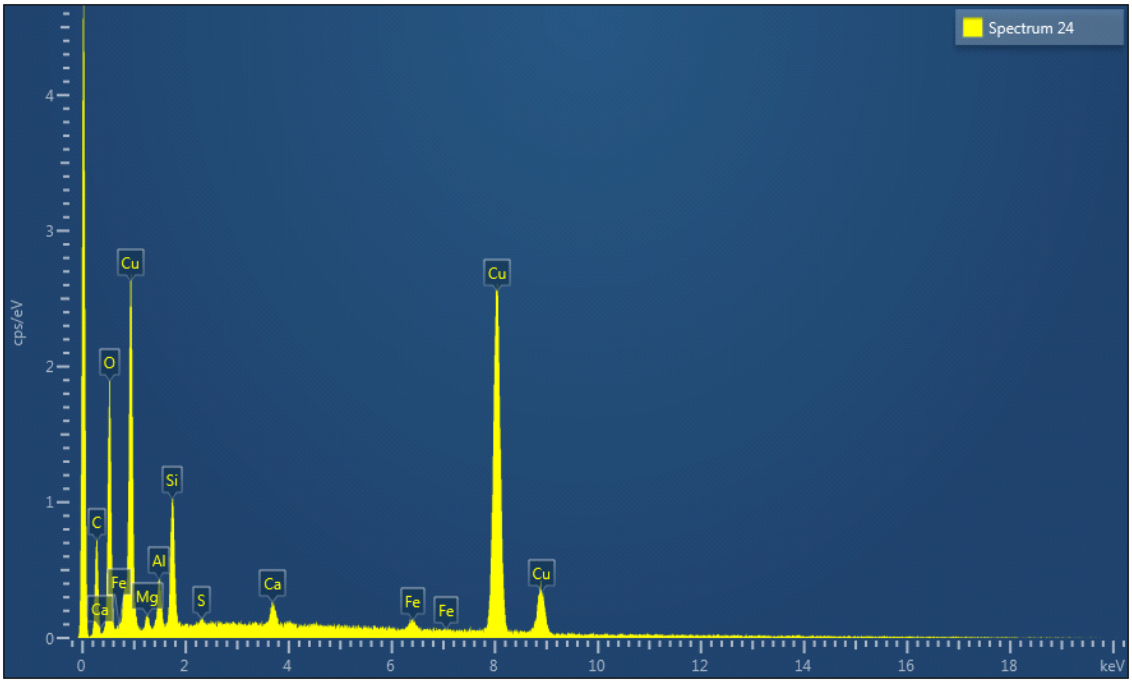

Figure 8.4c Chemical Spectra of area 24 in figure 8.4a.

From the images it can be concluded that the bentonite based particle is not porous. The CuO areas are porous and allow access to the CuO material inside the particle for reacting gases. The images do not show significant evidence of sintering due to the calcination process. Images of the particles were taken following the tests. The CU80B20 and Cu90B10 show similar features and morphology. The Cu60B40 particles, however, show more fragmented areas after the testing. The areas of CuO also seem to show altered morphology and less defined crystallinity. The pores evident in the images taken before the fluid bed tests are still evident in the images taken after the testing. However in the images taken after the testing, the pores are larger and less numerous, indicating a lower surface area of the CuO material.

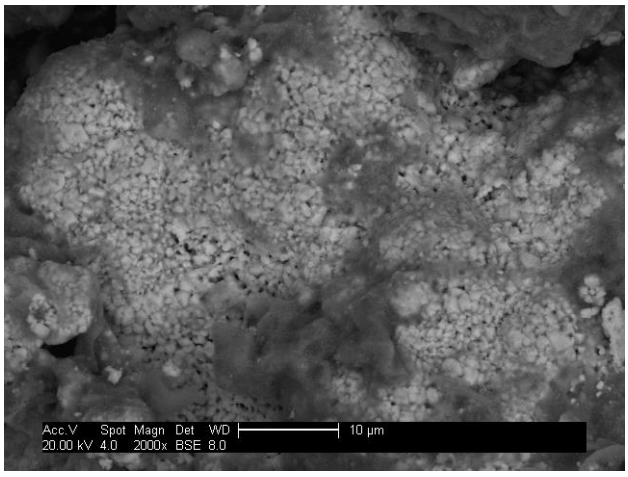

Figure 8.5 SFEG image of Cu60B40 berore fluid bed testing.

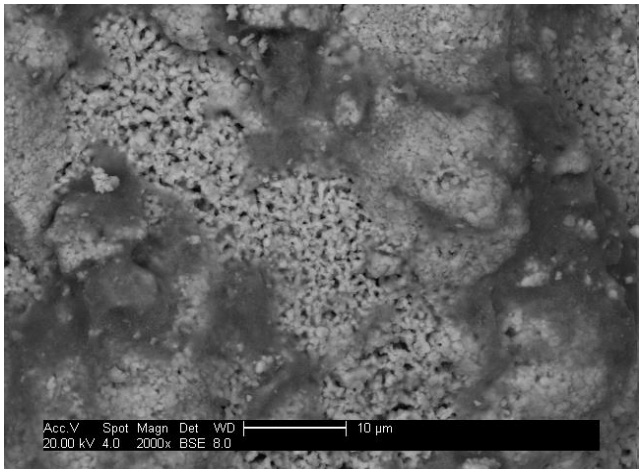

Figure 8.6 SFEG image of Cu80B20 before fluid bed testing.

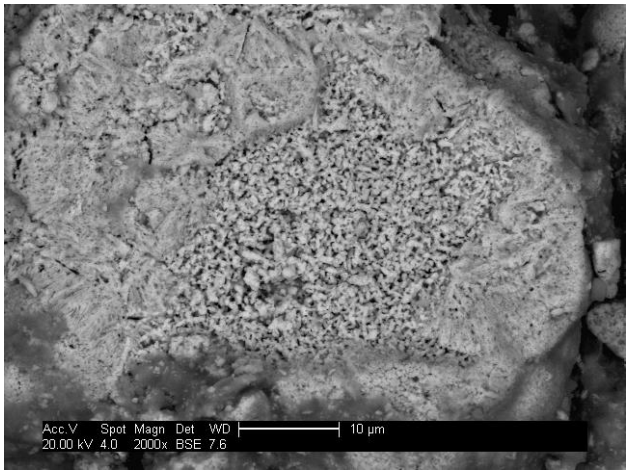

Figure 8.7 SFEG image of Cu90B10 before fluid bed testing.

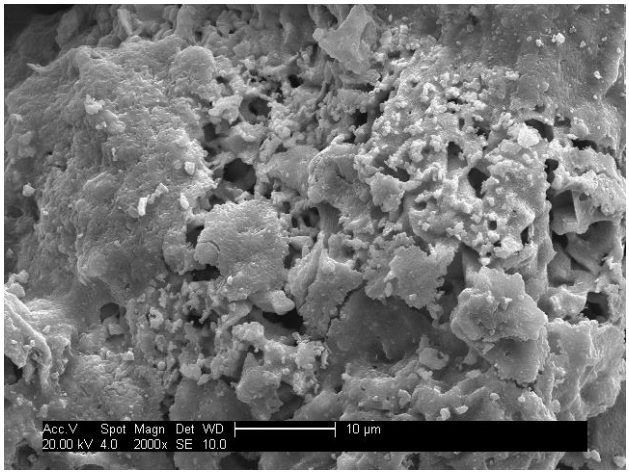

Figure 8.8 SFEG image of Cu60B40 after fluid bed testing.

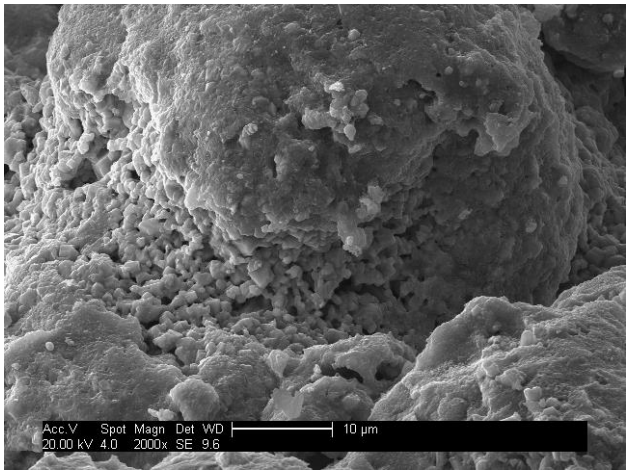

Figure 8.9 FEG image of Cu80B20 after fluid bed testing.

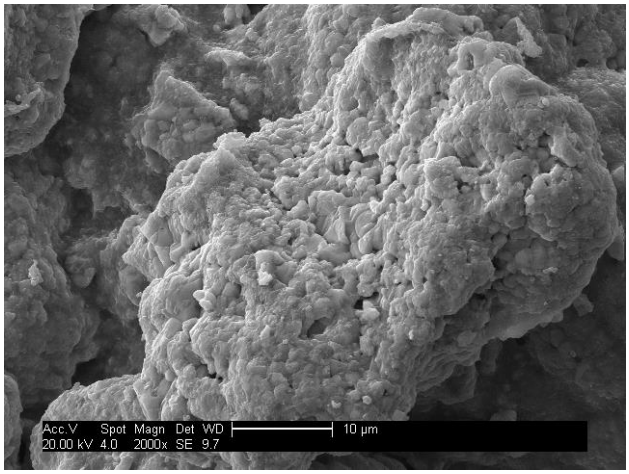

Figure 8.10 SFEG image of Cu90B10 after fluid bed testing.

8.3.3 XRD Testing

XRD testing was carried out on all three types of particles once they had been calcined, as part of the characterisation testing. As can be seen from the figures, The Cu60B40 particles contain CuO, as is to be expected. The results also show crystalline material in the bentonite. These particles contain SiO_2 in the crystobalite form, as well as $MgSiO_3$. The Cu80B20 particles show larger counts for CuO related peaks, and lower counts for peaks related to material in bentonite. This pattern continues in the Cu90B10 particles, which show larger counts for CuO, and lower counts for bentonite. This is to be expected as the Cu80B20 and Cu90B10 particle types contain less bentonite, as shown in the Research Method section.

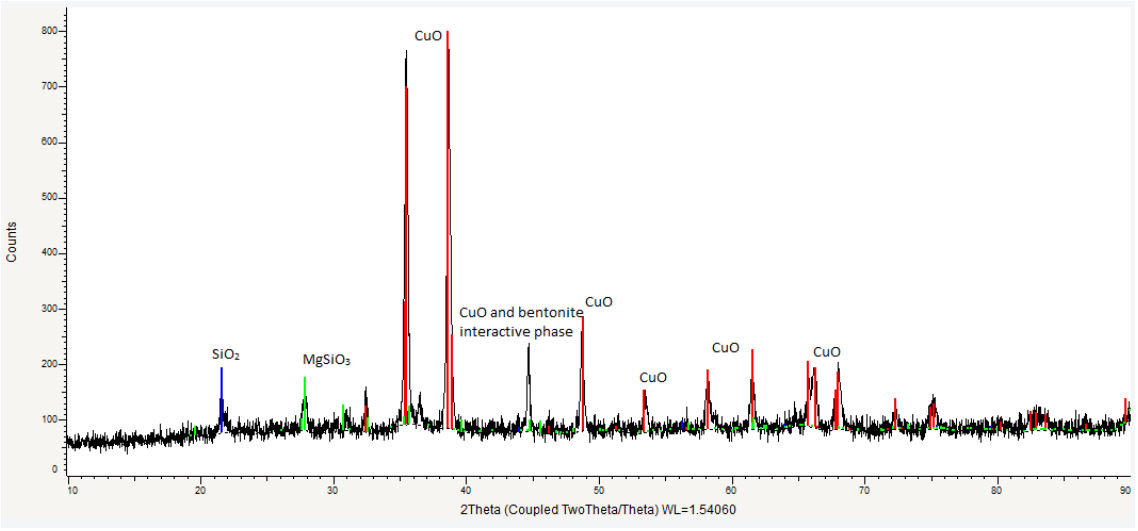

Figure 8.11 XRD results for Cu60B40 before fluid bed testing.

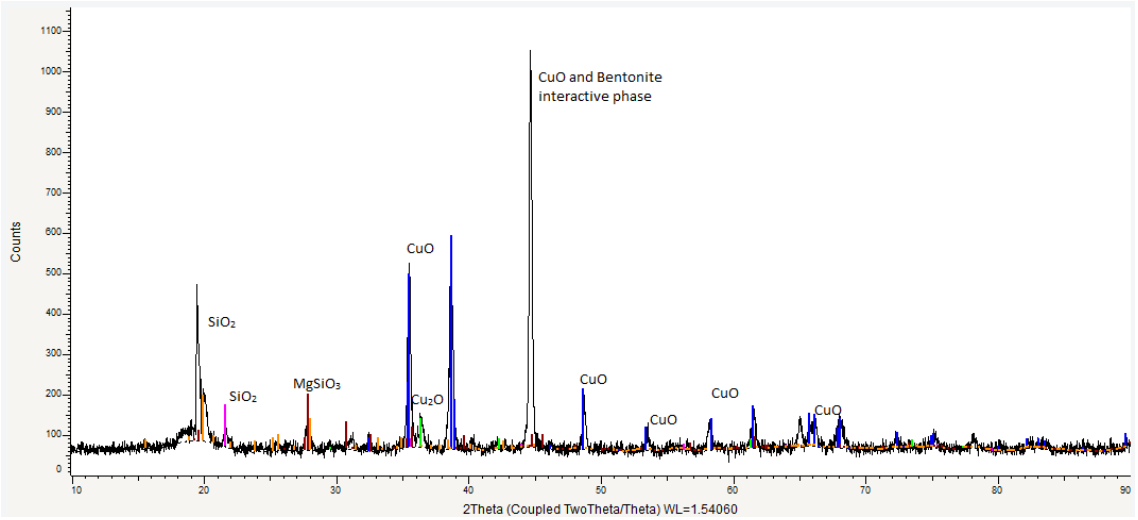

Figure 8.12 XRD results for Cu60B40 after fluid bed testing.

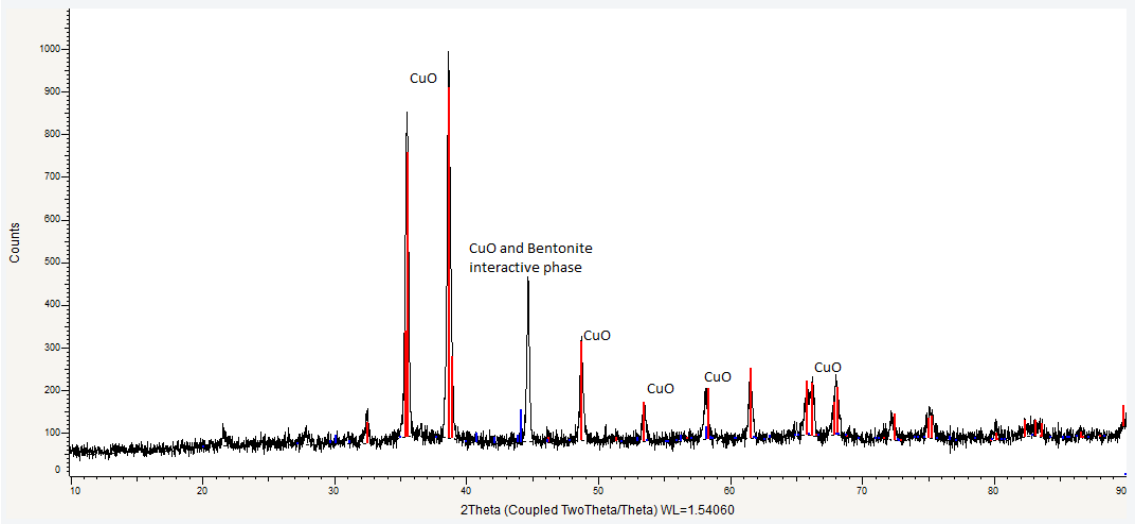

Figure 8.13 XRD results for Cu80B20 before fluid bed testing.

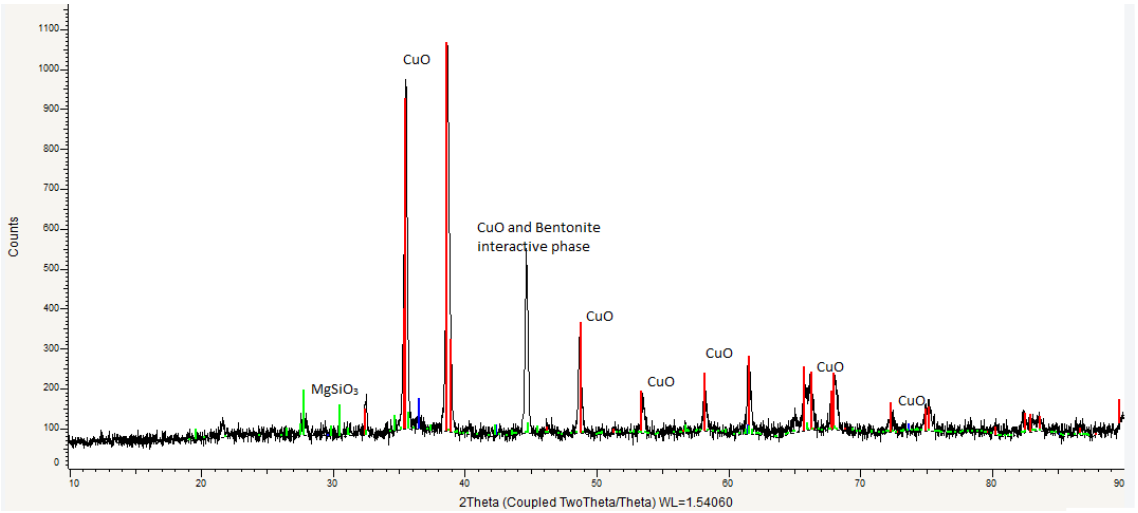

Figure 8.14 XRD results for Cu80B20 after fluid bed testing.

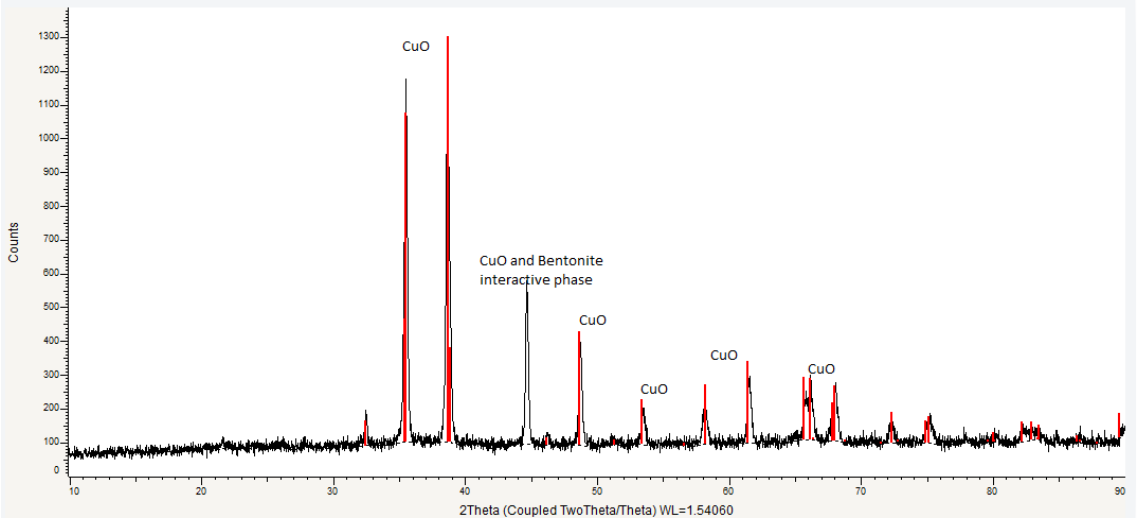

Figure 8.15 XRD results for Cu90B10 before fluid bed testing

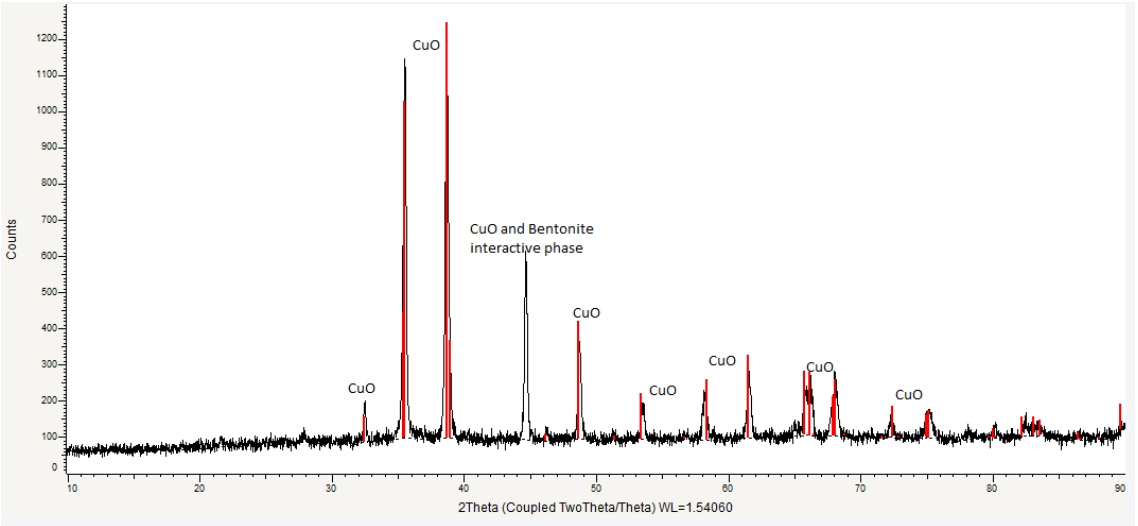

Figure 8.16 XRD results for Cu90B10 after fluid bed testing.

Additional XRD testing was carried out on particles after they had been subjected to the reduction and oxidation cycles in the fluid bed. The XRD test results for the Cu60B40, Cu80B20, Cu90B10 particles before fluid bed testing, and the same particles after testing are shown above in figures 8.11, 8.12, 8.13, 8.14, 8.15, and 8.16 respectively. The results for the Cu60B40 particles before and after fluid bed testing show largely similar peaks. However there is the notable addition of peaks

relating to Cu_2O. This confirms that the particles were reduced to Cu_2O during the cycles. However, the cycles ended in the reduction stage. The XRD counts of the respective peaks indicate a higher amount of CuO than Cu_2O present in the particles. This indicates that the particles were not able to reach significant conversion during the fluid bed testing. The XRD results for the Cu80B20 and Cu90B10 particles also show little difference between pre and post cycle testing. Both also show a very low amount of Cu_2O present in the particles, indicating an even smaller level of conversion for these particles. This corroborates the results found during the fluid bed testing. Additionally, the results show a peak around $2\theta=44^{o}$, in the spectra above. This is interpreted as an interactive, unreactive phase between the bentonite and copper oxide. This phase is least evident in the freshly calcined Cu60B40 particles, but is present in all the freshly calcined particles. It is also present in the results of the post cycling particles. In the Cu90B10 and Cu80B20 particles, this phase seems relatively unchanged, with the counts of the relevant peak unchanged. However in the XRD results of the Cu60B40 particles, this peak is much stronger, with much larger count number. This indicates that this interaction became more severe in these particles as they underwent reduction and oxidation cycles. This would explain the loss of performance of the Cu60B40 particles over progressive cycles

9 Discussion

9.1 TGA Results

This section will discuss the performance of the Cu90B10 particles in TGA testing. The particles were able to achieve full conversion in reduction. This is to be expected with CuO based particles. CuO is reactive with CO and the reaction will reach full conversion of the limiting reactant. The reduction reaction here is also exothermic, and may cause a small increase in temperature of the equipment. The enthalpy change for the reaction is -126.9 kJ/mol CO. The conversion data do indicate that the production method was able to reliably achieve an accurate proportion of constituents, with a slight excess of CuO in sample carried out at $900^{o}C$, as this sample reached X=1.1 in reduction

conversion. Full reduction was achieved in 2 minutes at the 10th cycle. This time does increase over the cycles, but is a good time when considered amongst other oxygen carrier particles in literature. The reduction under N_2 was only able to achieve around X=0.1 over the 2 minute period even in the best performing 900°C condition. This did deteriorate from X=0.2 over that period. The oxidation from Cu to Cu_2O is reliable, and fairly quick. In all samples it was achieved by 6 minutes in the 10th cycle, however it is expected that it would become slower if more cycles are carried out. However, the oxidation past this point is not so promising. In the tests carried out at 940°C, by the 10th cycle, the particles were not able to oxidise past X=0.5, which corresponds to Cu_2O. This would render these particles unable to carryout CLOU at 940°C, as oxidation and reduction between the CuI and CuII oxidation states is the fundamental process in CLOU. However, at lower temperatures, oxidation past X=0.5 is achieved. The rate of oxidation is an issue. After 10 minutes of oxidation, the particles achieve highest oxidation at 900°C, which is X=0.7. Achieving higher oxidation conversion in the air reactor means that the particles provide a larger oxygen transport capacity. The rate of oxidation conversion indicates that the particles will require a long residence time in the air reactor in order to provide acceptable oxygen transport capacity. The optimal temperature is 900°C. This temperature shows the highest and fastest oxidation conversion, even when allowing for the slightly high proportion of CuO in the particles.

This section considers the results of the Cu80B20 TGA testing. When looking at the maximum degree of conversion, it can be seen that the particles achieve X=1 conversion in reduction. This indicates that the particles contain a reliable proportion of CuO material. This reinforces the information from the Cu90B10 testing. At 940°C at the 10th cycle, there is no oxidation past X=0.5, meaning that the particles do not oxidise to CuO. This is similar to the Cu90B10 particles and means that the particles are not appropriate for use in CLOU at 940°C. In the 10th cycle, the particles are able to oxidise to X=0.5 at 920°C, 900°C and 880°C within 3 minutes, with the particles at 880°C reacting the fastest. The oxidation beyond

this is much slower, requiring around 12 minutes to reach X=0.7 at each temperature. This indicates that the particles would need a long residence time in the air reactor to allow acceptable oxidation conversion, and therefore oxygen transport capacity. The reduction of all particles reaches X=1 conversion under CO flow. As discussed above, this is to be expected for CuO based particles. The time for this reduction is around 2 minutes for all types of particles, with the particles operating faster at 920^{o}C. At 880^{o}C, the particles reduce very slowly under N_2 flow. This behaviour is consistent from the first cycle. At 920^{o}C, the reduction under N_2 flow is faster, but at 920^{o}C, the particles reduce fastest under N_2 flow. Even at the best performance, the particles are capable of only X=0.2 in 2 minutes. In the first cycles, the particles were able to achieve X=0.2 in about 90 seconds, meaning that progressive cycles result in deterioration of performance.

The performance of the Cu60B40 particles follows the trend of the previous 2 particle types. At 940^{o}C, the particles are unable to oxidise to CuO. This means that at this temperature, the particles are unsuitable for CLOU. The performance of the reduction in N_2 is best at 920^{o}C. The particles are capable of X=0.2 in 90 seconds at cycle 10 under these conditions. At 900^{o}C and 880^{o}C, the rate of reduction in N_2 is lower. At 920^{o}C, the reduction in N_2 does deteriorate from X=0.2 in 1 minute in the first cycles to 2 minutes in the 10th cycle. The reduction in CO performs well across all temperatures for these particles. As with the other particles, full conversion is achieved at a good rate. This again indicates a reliable proportion of CuO and bentonite in the particles. The particles are able to achieve full reduction in approximately 2 minutes at all temperatures, and from the first cycles to the 10th cycle. At 920^{o}C, 900^{o}C, and 880^{o}C, the particles can oxidise to X=0.7, approaching X=0.8. The oxidation rate is best at 880^{o}C, and slowest at 920^{o}C. All are able to reach X=0.7 in 6 minutes. At 880^{o}C. The oxidation performance deteriorates only slightly from the first cycles to the 10th cycle. At 920^{o}C, there is more significant deterioration from the early cycles to the 10th cycle. Considering the oxidation performance in terms of industrial application, it allows for lower residence time that the Cu80B20 and Cu90B10 particles,

however it still requires 5 to 6 minutes. The optimal temperature considering a balance between oxidation and reduction performance appears to be 900^{o}C.

Looking at all particles relative to each other. The optimal performance for the Cu90B10, Cu80B20, and Cu60B40 particles are 900^{o}C, 920^{o}C, and 900^{o}C respectively. This section will discuss the oxidation and reduction curves for each particle type at its optimal performance temperature, as shown in figures 8.1 and 8.2 above. The best performance for both oxidation and reduction is Cu60B40. The oxidation performance for the Cu60B40 particles shows best performance with a good rate to X=0.7. Both the other two types of particle only show a good rate to about X=0.5, then the rate slows significantly. This can be partially explained by the equilibrium concentration of oxygen at the surface of the copper compound at these temperatures. At lower temperature there is a lower equilibrium concentration of oxygen. The concentration of oxygen the oxidation condition of these tests is 5%. At lower temperature the higher difference between the supplied oxygen concentration and the equilibrium concentration provides the driving force for oxidation (Clayton et al., 2014). The difference between each particle type cannot be explained by this, as the equilibrium concentration is the same for each particle type. As shown in previous studies (Adanez-Rubio, I. et al., 2011, Adanez-Rubio, I. et al., 2012, Gayan et al., 2012), particles prepared with a variety of support materials, such as silica, sepiolite, zirconia, and magnesium-alumina, are able to reach full conversion in both reduction and oxidation within 2 minutes in a TGA. The results here match these results in terms of reduction. This means that bentonite performs as well in reduction as these support materials. However, the particles supported on bentonite were not able to reach full oxidation conversion. This means that bentonite is not as effective a support material as magnesium-alumina or silica shown in the study by Adanez-Rubio et al.

The difference between the performances of these particles can be explained in a different way. These figures are taken from the 10th cycle of oxidation and

reduction for the tests. The 10th cycle for the Cu60B40 particles has not deteriorated significantly from the first cycles. However, for both Cu80B20 and Cu90B10 particles, there is significant deterioration in performance from the first cycles to the 10th cycle. This adds to the conclusion here that Cu60B40 particles are the best performing, by showing that as the number of cycles increases, these particles will hold their performance much more effectively than the Cu80B20 and Cu90B10 particles. This means that there will be less of a need for a make-up flow of particles, as well as requiring less residence time in the air reactor overall. All the particles show good performance in reduction under CO. However, the Cu60 B40 particles show the best reduction performance in the N_2 purge phase. They show the highest change in conversion over the 2 minute period. However, even the Cu60B40 particles show deterioration from the first cycles to the 10th cycles.

These TGA tests show that sintering will take place when using fuel. This is shown by the deterioration in performance over progressive cycles. The tests have revealed that the 3 different types of particle are not able to carry out CLOU behaviour at 940^{o}C. The tests have revealed that the Cu60B40 and Cu90B10 particles also experience significant sintering at 920^{o}C when carrying out cycles with fuel. Due to this, the best performance for these particles is at 900^{o}C. The Cu80B20 particles show quite similar behaviour between 900^{o}C and 920^{o}C. The sintering was not shown to be significantly higher for these particle sat 920^{o}C. However, the sintering was found to be lowest with the Cu60B40 particles, which are able to maintain their performance the best when being used with fuel.

9.2 Fluid Bed Results

When interpreting the data for the fluid bed tests, let us start by looking at the effect of temperature. The change in oxygen concentration in both reduction and oxidation tends to be slower at lower temperature. This indicates faster reaction

rate in both cases, and a greater degree of conversion. In oxidation, this general trend can be explained by the difference between the oxygen partial pressure at equilibrium, and that in the atmosphere at the surface of the CuO. The greater the difference, the greater the driving force for oxidation. At 940^{o}C, CuO has a larger equilibrium partial pressure of oxygen at the surface of the metal, and as the oxygen concentration used in these tests is 5%, this is close to the equilibrium concentration at 940^{o}C. This means the rate of oxidation is expected to be lower at 940^{o}C, and this is true across all the particle types. However, in reduction, the difference between atmospheric and equilibrium oxygen concentration should be greater at higher temperature. In fact, it is found that the reduction rate for all these particles is greater at lower temperature, which goes against our expectations here.

The oxygen carrier particle composition has a large effect. The different compositions here are Cu60B40, produced with 60%wt CuO, Cu80B20, produced with 80%wt CuO, and Cu90B10, produced with 90%wt CuO. In all cases, the balance weight percentage consists of bentonite clay. It is an established fact that including support material helps in the prevention of sintering, and oxygen carrier material degradation with prolonged use. However, it has also been noted that bentonite can react with carrier materials and cause sintering (Manovic & Anthony 2009). With these two potentially competing effects here, it is necessary to determine whether increased bentonite content has a beneficial or detrimental effect. From the data, it can be seen that in almost every cycle, increased bentonite content results in a slower rate of oxygen concentration change in both oxidation and reduction. This indicates that increased bentonite content has a beneficial effect and improves oxygen carrier performance, allowing for increased conversion in both reduction and oxidation. This indicates that the general support function of the bentonite outweighs any effect from reacting with the CuO, or any sintering. This trend is not as distinct between the Cu80B20, and Cu90B10 particles. These particles often show the

same performance, and under some conditions, Cu90B10 performs better than Cu80B20. There is no significant trend between these 2 particle types.

When interpreting the effect of the number of cycles of the performance of the particles, there is a less clear outcome. For the Cu90B10 particles, there is only a clear trend in the 880^{o}C, where increasing cycle number slightly decreases performance. The data for Cu80B20 particles show similar results. At higher temperature, there is no difference between the cycles. At 880^{o}C, there is slight reduction in performance over the cycles. The Cu60B40 particles show more a significant effect with increasing number of cycles. This effect is the most significant at low temperature, as with the other particle types, but is also present at 920^{o}C. At 940^{o}C, there is no longer any effect. There is a compounding effect of temperature with the number of cycles carried out. Where there is already poor performance in the high temperature cycles, the performance is bad enough that there is no measured deterioration in performance. Where performance in better, in the low temperature tests, there is room for deterioration in particles, and an effect is seen. It is important to note that for the Cu90B10 particles, the 880^{o}C and 900^{o}C tests were performed after the 920^{o}C and 940^{o}C tests, and had already been through 40 cycles. Let us consider the best performing particles, those of CU60B40 at low temperatures. These particles show a marked difference in performance from the Cu80B20 and Cu90B10 particles in the early cycles. However this difference reduces with increasing cycle number, and in the 10th cycle, the performance of the Cu60B40 particles is similar to that of the other particles.

The very low level of conversion achieved in these tests is interesting. As seen in the TGA testing, the Cu60B40 particles were able to achieve reduction conversion of X=0.2 at 900^{o}C during the 2 minute nitrogen purge. This conversion value was calculated assuming CO as reducing gas, meaning it accounts for reduction to metallic Cu. As the reduction seen in that purge phase was CLOU behaviour, it would be appropriate to examine the conversion in terms of reduction to Cu_2O. The maximum reduction conversion to Cu_2O is half that for

the conversion to Cu. This means we can simply double the value of X to show the conversion that the particles achieved in relation to CLOU.

So in terms of CLOU, the Cu60B40 particles achieved X=0.4 reduction conversion during the purge phase. This is 10 times higher than the X=0.04 reduction conversion achieved by the same Cu60B40 particles in the fluid bed testing. As mentioned in the Results section, the flow of the gas through the particles may have played a role here. Agglomeration is a known problem for copper and copper oxide based oxygen carriers (Adanez et al., 2012). The temperatures used here have been known to cause agglomeration in previous studies. Agglomeration was observed in these tests. When the reaction vessel was emptied, clumps of agglomerated material was found. This is likely to have caused the gas flowing through the vessel to move though channels between the clumps, rather than between each particle. This would mean that the reacting gases did not come into contact with the majority of particles.

Previous studies (Peterson. S, B. et al., 2013, Adanez-Rubio, I. et al., 2011) did attempted fluidisation testing in a fluidised bed with CuO based particles. These studies report agglomeration during fluidisation, which led to low amounts of oxygen released during reduction. This indicates that the problems found in this study are not unique, but are faced by other researchers attempting to study CuO based materials. These studies also suffered from low oxygen release during reduction, and corresponding low oxidation during oxidation phases. This is not universal, however. The study by Gayan et al., shows that CuO based particles, here supported on zirconia, were able to be fluidised. These particles were able to reach good rates for release of oxygen in the reduction phase. This indicates that it is possible to produce particles based on CuO which are able to show good fluidisation characteristics.

When considering all factors involved in the performance of these particles, the number of cycles carried out is the least significant. There is little sintering in these particles caused by repeated cycling. However, the reduction here does not include any fuel. The effect of using fuel to reduce the particles is discussed in the review of the TGA data. The particles with the composition that performed

best were the Cu60B40 particles. Like other carrier materials, it appears that bentonite does has a negative effect on the particles. However, this effect is less severe than simply leaving the copper material with little or no support. The effect of temperature is to reduce the ability of the particles to carry out CLOU as temperature increases. This is true for oxidation, as expected, and also for reduction.

10 Conclusion

The crushing strength testing indicates that the Cu60B40 particles would have the required strength to operate in a fluid bed rig with acceptably low elutriation of fine particles. This is supported by the very low loss of material from the fluid bed testing. This result is supported by the improved crushing strength found for the particles after the reduction and oxidation cycles in the fluid bed tests. The SEM and SFEG imaging indicates little change to the Cu80B20 and Cu90B10 particles, but does indicate changes to the Cu60B40 particles. The XRD results support this. The XRD results for the Cu80B20 and Cu90B10 particles do not show significant difference before and after the fluid bed tests, including a very low presence of Cu_2O after the fluid bed tests. However, the Cu60B40 particles do show changes between the particles before and after the fluid bed testing. Notably the XRD results show the presence of Cu_2O in these particles after fluid bed testing. The results also show that the particles reacted with the bentonite support and formed an irreducible phase in the particles. This phase did negatively affect the performance of these particles.

The fluid bed tests show that the effects of the bentonite as support material are more complex. The Cu80B20 and Cu90B10 particles showed very poor performance in the fluid bed tests. The XRD results even suggest that almost no CU_2O was produced in the CU90B10 particles, with only very little being produced in the Cu80B20 particles. This is supported by the fluid bed test results,

which show an extremely small amount of oxygen being released by these particles during the tests. This shows that the particles need effective support in order to function as oxygen carrier particles. These results suggest that the calcination process may have been sufficient to render the CuO inactive and prevent it from carrying out CLOU activity. The Cu60B40 particles did show better performance and oxygen release, although still low. This is supported by the XRD results, which do show the presence of Cu_2O in the particles after the fluid bed tests. In this case the bentonite was able to give effective support to the CuO and retain some activity during the calcination process. The fluid bed tests also show that increasing temperature is detrimental to the performance of all particles produced here.

As mentioned in the Discussion section, agglomeration is a known problem for copper and copper oxide based oxygen carriers. Agglomeration of the Cu60B40 particles was less severe than the other two particle types. Agglomeration was still likely in these particles and lead to smaller scale clumps forming. Agglomeration of the Cu80B20 and Cu90B10 particles was severe and did cause defluidisation of the particles, indicated by a large pressure drop across the bed. In the Cu60 B40 particles, this agglomeration was not so severe, indicating that the bentonite support did provide some protection against this effect. However, agglomeration is likely to have caused a reduction in the mixing of the gas amongst the bed. This would lead to low gas flow in parts of the bed and low availability of oxygen to the particles in agglomerated areas. This would reduce the total reduction of the particles, by allowing air to accumulate in these areas without being driven out by the flow of gas, and reducing the driving force of reduction. It would also affect oxidation by simply reducing the availability of oxygen to particles in agglomerated areas.

The TGA results show much improved performance of the particles. The particles were able to reach full reduction conversion quickly and reliably when using CO as reducing gas. This was true of all particles used and at all temperatures. The fluid bed testing indicated that, particularly for the Cu80B20 and Cu90B10

particles, oxidation and CLOU reduction reactivity in an inert atmosphere, between CuO and Cu_2O, is significantly affected by progressive cycles. The TGA results indicate that reduction to Cu by a reducing gas, in this case CO, is not as badly affected for any of the particles tested. The 2-minute nitrogen purge period after each oxidation stage shows CLOU activity for some of the particles tested. The Cu60B40 particles show the best performance here, with a change of around X=0.2 at optimum conditions. The Cu80B20 particles do show some CLOU activity, giving around X=0.1 change over the purge period. However, after the first cycle, the Cu90B10 particles show very little CLOU activity, close to no conversion change. The oxidation stages also show that the Cu60B40 particles clearly have the best performance. These results follow the trend of the fluid bed tests, however the small number of particles appear to reach much more significant conversion in the TGA than the larger samples used in the fluid bed tests. This highlights the difficulty the particles had in achieving high reduction conversion in the fluid bed testing, indicating poor mixing of the flowing gas. This suggests that the particles supported on bentonite are not well suited to fluidisation and may be better suited to packed bed reactor use.

The good reactivity of the reduction with CO, compared with the CLOU reduction in N_2 shows that the particles will react with reducing gas, such as that from volatiles in coal, before undergoing a CLOU reaction. This means that if the particles are used in a CLOU reactor, they will have to be used in large excess to allow enough oxygen from the reduction from CuO to Cu_2O to react with the volatiles from the solid fuel, and to be released as gaseous oxygen to react with the solid fuel. These particles should also contain a significant proportion of bentonite, such as the Cu60B40 particles produced here, to ensure sufficient stability of the particles. However, these large solids inventory of particles would not be needed if used with gaseous fuel such as syngas or methane, rather than solid fuel.

All the particles produced here are reasonably low cost materials and production methods that were relatively simple and easy. The particles show that a high proportion of bentonite should be used in producing particles to ensure sufficient strength in the particles to survive full-scale fluidisation conditions. This is also necessary to ensure the particles maintain stability and the ability to undergo CLOU activity. The particles with lower bentonite content allow for higher oxygen transport capacity. This is shown by the oxygen carrying capacity in CLOU of Cu90B10 particles, compared to Cu60B40 particles, which is 0.9 $kgO_2/kgOC$, compared to 0.06 $kgO_2/kgOC$ respectively. However the particles with low support content lose activity very quickly, as shown by Tables 8.1c and 8.3c. Cu60B40 particles maintain $1.0x10^{-3}$ $mgO_2/mgOC.s$ reliably at 940^{o}C, where-as Cu90B10 particles go from $9.2x10^{-4}$ $mgO_2/mgOC.s$ to $7x10^{-4}$ $mgO_2/mgOC.s$ at 940^{o}C. This behaviour restricts the use of low support content particles as oxygen carriers. These particles also do not show good fluidisation behaviour, which restricts their use in full-scale reactors. These results do not support the findings of Tian et al (Tian et al., 2008), who also produced copper-based particles by a mechanical mixing method. The TGA results do support the positive findings of that work; however it is the fluid bed tests here which do not show the positive results. The difference is that the testing in that study looked at the particles with a mixture of CO and H_2 in the reduction phase, whereas this study used the fluid bed tests to look at pure CLOU activity. The reduction of copper based particles with reducing gas (e.g. natural gas, methane, carbon monoxide or syngas) shows good performance, due to the reactivity of copper with these gases. However, CLOU activity of particles using bentonite as support was inhibited.

There are several potential ways of moving forward with additional studies, based on the data gathered here. While the fluid bed test results shown here are not promising, the study by Gayan et al., 2012 shows that CuO based particles with good fluidisation properties are possible. Additional testing could be carried out with a range of fluidisation conditions to determine if conditions exist where the particles can be more effectively fluidised. Another potential option for oxygen

carrier particles is to use a cement, such as high alumina cement as support. This would fulfil the requirement of a low cost, readily available material. It would also allow particles to be produced by granulator, being a relatively low cost production method. Use of high alumina cement would reduce impurities in the cement that could react with the CuO and reduce activity. There has been some investigation of cement supported particles(Tian et al., 2015), (Xu et al., 2013) which support this suggestion. The studies shows low agglomeration of copper-based particles supported on cement.

REFERENCES

Abad, A. et al., 2007. Mapping of the range of operational conditions for Cu-, Fe-, and Ni-based oxygen carriers in chemical-looping combustion. *Chemical Engineering Science*, 62, 533–549.

Adanez, J. et al., 2012. Progress in chemical-looping combustion and reforming technologies. *Progress in Energy and Combustion Science*, 38, 215–282.

Adánez, J. et al., 2006. Chemical Looping Combustion in a 10 kW th Prototype Using a CuO/Al2O3 Oxygen Carrier: Effect of Operating Conditions on Methane Combustion. *Industrial & Engineering Chemistry Research*, 45, 6075–6080.

Adánez-Rubio, I. et al., 2011. Development of CuO-based oxygen-carrier materials suitable for Chemical-Looping with Oxygen Uncoupling (CLOU) process. *Energy Procedia*, 4, 417–424.

Adánez-Rubio, I. et al., 2012. Evaluation of a spray-dried CuO/MgAl 2O 4 oxygen carrier for the chemical looping with oxygen uncoupling process. *Energy and Fuels*, 26, 3069–3081.

Adánez-Rubio, I. et al., 2014. Kinetic analysis of a Cu-based oxygen carrier: Relevance of temperature and oxygen partial pressure on reduction and oxidation reactions rates in Chemical Looping with Oxygen Uncoupling (CLOU). *Chemical Engineering Journal*, 256, 69–84.

Arjmand, M. et al., 2013. ZrO2-Supported CuO Oxygen Carriers for Chemical-Looping with Oxygen Uncoupling (CLOU). *Energy Procedia*, 37, 550–559.

Berguerand, N. & Lyngfelt, A., 2008. Design and operation of a 10 kWth chemical-looping combustor for solid fuels - Testing with South African coal. *Fuel*, 87, 2713–2726.

Bernstein, L. et al., *Climate Change 2007 Synthesis Report*,

Cao, Y. & Pan, W., 2006. Investigation of Chemical Looping Combustion by Solid Fuels . 1 . Process Analysis. *Combustion*, 8, 1836–1844.

Chitester, D.C. Kornosky, R.M., Characteristics of fluidization at high pressure 1984. *Chem Eng Sci,* 39, 253-261

Chuang, S.Y. et al., 2008. Development and performance of Cu-based oxygen carriers for chemical-looping combustion. *Combustion and Flame*, 154, 109–121.

Clayton, C.K., Sohn, H.Y. & Whitty, K.J., 2014. Oxidation kinetics of Cu2O in oxygen carriers for chemical looping with oxygen uncoupling. *Industrial and Engineering Chemistry Research*, 53, 2976–2986.

Corbella, B.M. et al., 2006. Characterization and performance in a multicycle test in a fixed-bed reactor of silica-supported copper oxide as oxygen carrier for chemical-looping combustion of methane. *Energy and Fuels*, 20, 148–154.

Emerson, W.W., 1962. The Swelling of CA-Montmorillonite due to Water Absorption. *Journal of Soil Science*, 13, 40-45.

De Diego, L.F. et al., 2004. Development of Cu-based oxygen carriers for chemical-looping combustion. *Fuel*, 83, 1749–1757.

Gayán, P. et al., 2012. Development of Cu-based oxygen carriers for Chemical-Looping with Oxygen Uncoupling (CLOU) process. , 96, p226–238.

Hai-bo, Z. et al., 2008. NiO / NiAl 2 O 4 oxygen carriers prepared by sol-gel for chemical-looping combustion fueled by gas. , 36, 898–905.

Hemingway, J. & Michaels, C., 2012. Electricity generation and supply figures for Scotland , Wales , Northern Ireland and England , 2008 to 2011, 50–58.

Imtiaz, Q., Broda, M. & Müller, C.R., 2014. Structure-property relationship of co-precipitated Cu-rich, Al2O3- or MgAl2O4-stabilized oxygen carriers for chemical looping with oxygen uncoupling (CLOU). *Applied Energy*, 119, 557–565.

Jerndal, E. et al., 2010. Investigation of NiO/NiAl2O4 oxygen carriers for chemical-looping combustion produced by spray-drying. *International Journal of Greenhouse Gas Control*, 4, 23–35.

Jerndal, E., Mattisson, T. & Lyngfelt, A., 2006. Thermal analysis of chemical-looping combustion. *Chemical Engineering Research and Design*, 84, p795–806.

Kunii, D., and Levenspiel, O., 1991. 'Fluidization Engineering' *Butterworth Heinemann.*

Lewis, W.K., Gilliland, E.R., Sweeney, W.P., 1951, “Gasification of carbon: metal oxides in a fluidized powder bed“, Chemical Engineering Progress 47(5), 251-256.

Manovic, V. & Anthony, E.J., 2009. Screening of binders for pelletization of CaO-based sorbents for CO_2 capture. *Energy and Fuels*, 23(10), p4797–4804.

Mattisson, T. et al., 2007. Chemical-looping combustion using syngas as fuel. *International Journal of Greenhouse Gas Control*, 1, p158–169.

Monazam, E.R. et al., 2012. Kinetics of the Reduction of CuO/Bentonite by Methane (CH_4) during Chemical Looping Combustion. *Energy & Fuels* 26 (5), 2779-2785

Peterson, S, B. et al, 2013, Characteristics and Performance of a Novel SiO_2-Supported Oxygen Carrier Prepared CuO and β-SiC

Rydén, M. et al., 2014. CuO-based oxygen-carrier particles for chemical-looping with oxygen uncoupling - Experiments in batch reactor and in continuous operation. *Industrial and Engineering Chemistry Research*, 53, 6255–6267.

Tian, H. et al., 2008. Chemical-looping Combustion of Coal-derived Synthesis Gas Over Copper Oxide Oxygen Carriers. , 12, 3744–3755.

Tian, H. et al., 2009. Effect of Hydrogen Sulfide on Chemical Looping Combustion of Coal-Derived Synthesis Gas over Bentonite-Supported Metal - Oxide Oxygen Carriers. , *Ind. Eng. Chem. Res.*, *48* 8418–8430

Tian, X. et al., 2015. Performance of cement decorated copper ore as oxygen carrier in chemical-looping with oxygen uncoupling. *International Journal of Greenhouse Gas Control*, 41, 210–218.

Wilcox, J., 2012. 'Carbon Capture' *Springer*

Wu, Y. et al., 2012. Modified lime-based pellet sorbents for high-temperature CO 2 capture: Reactivity and attrition behavior. *Fuel*, 96, 454–461.

Xu, L. et al., 2013. Experimental study of cement-supported CuO oxygen carriers in chemical looping with oxygen uncoupling (CLOU). *Energy and Fuels*, 27, 1522–1530.

Yu, C.H., Huang, C.H. & Tan, C.S., 2012. A review of CO2 capture by absorption and adsorption. *Aerosol and Air Quality Research*, 12, 745–769.

Zhou, Z. et al., 2014. Continuous regime of chemical looping combustion (CLC) and chemical-looping with oxygen uncoupling (CLOU) reactivity of CuO oxygen carriers. *Applied Catalysis B: Environmental*, 166, 166-167 .

Appendix 1 Fluid Bed Test Data

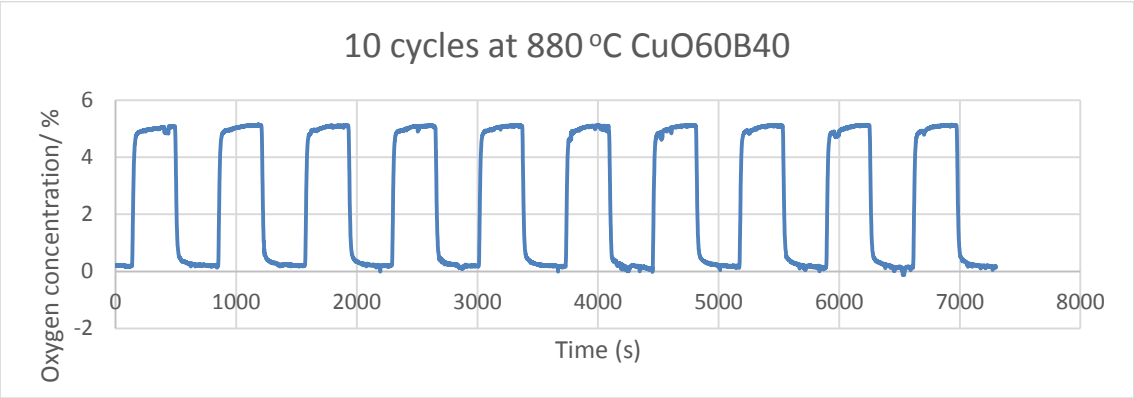

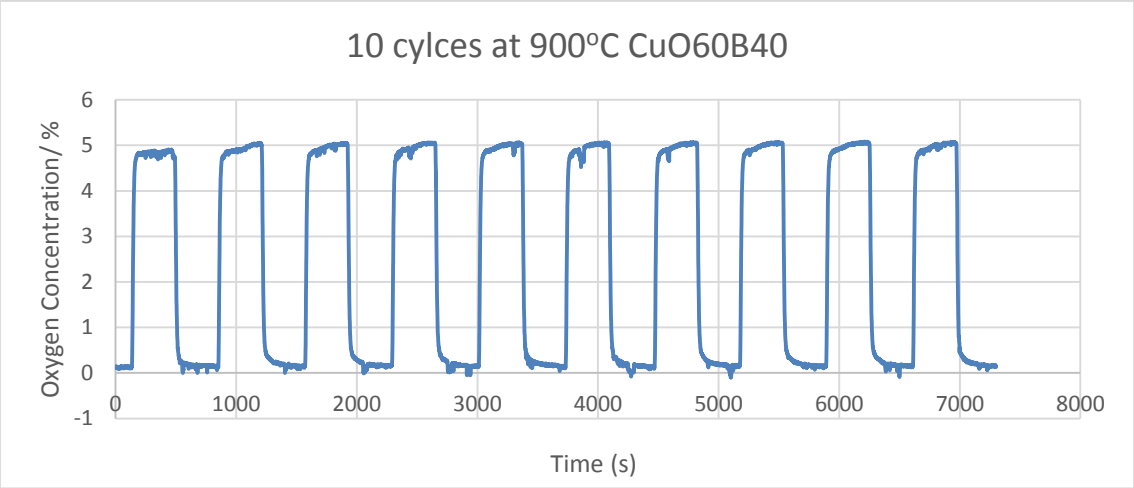

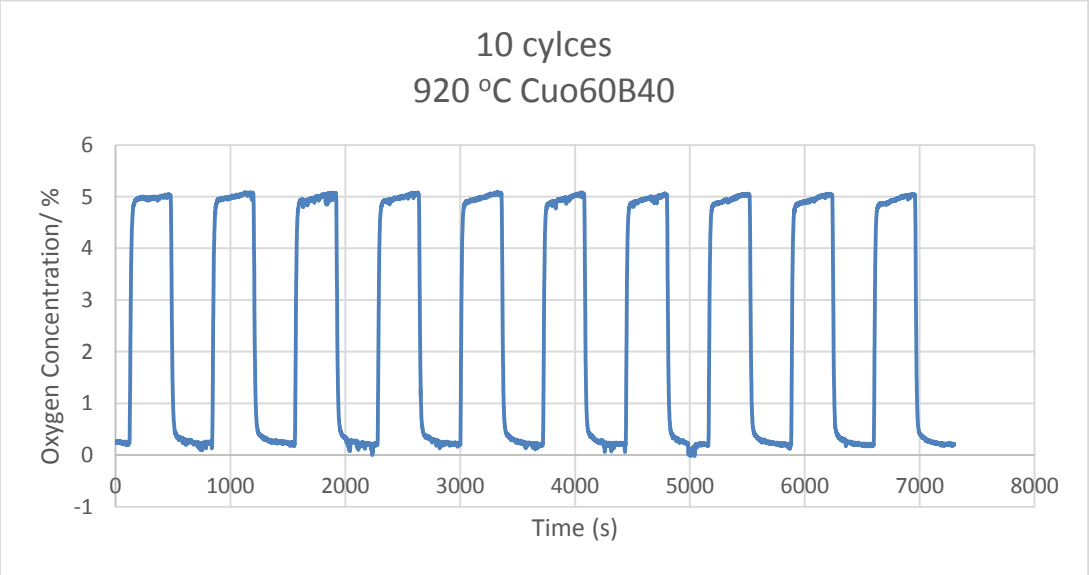

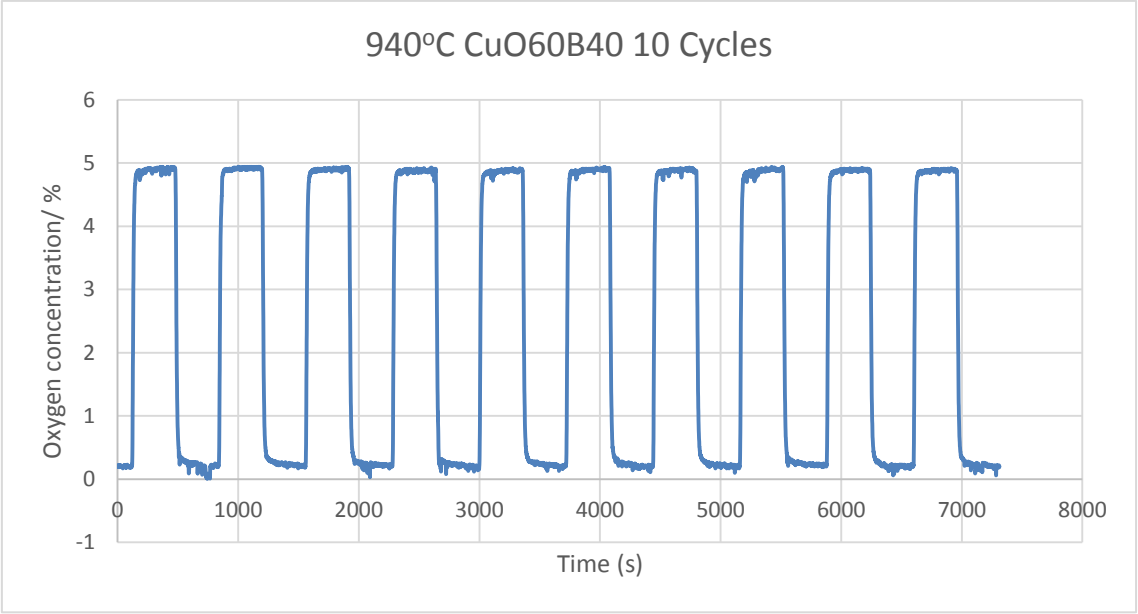
940°C CuO60B40 10 Cycles
Oxygen concentration/ %
6
5
4
3
2
1
0
-1
0
1000
2000
3000
4000
5000
6000
7000
8000
Time (s)

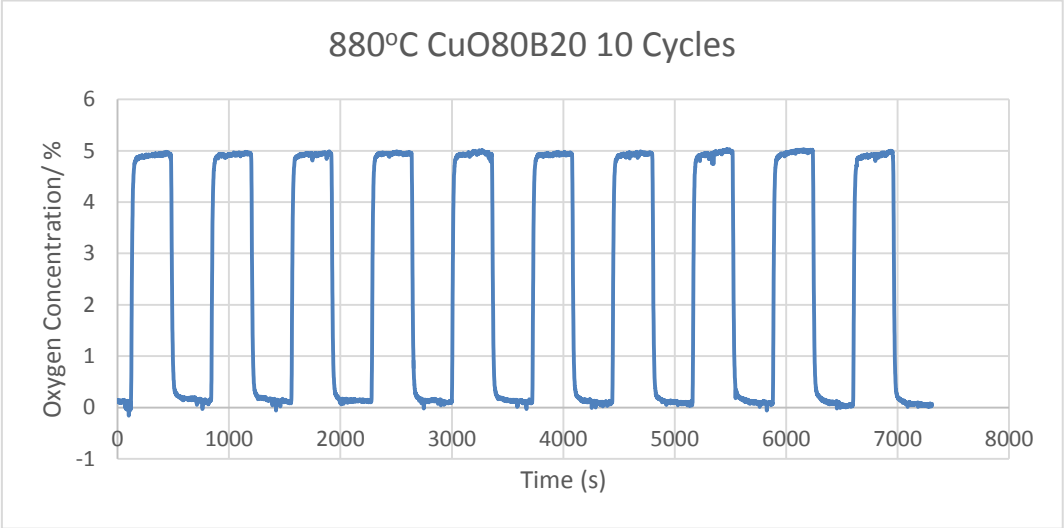
880°C CuO80B20 10 Cycles
Oxygen Concentration/ %
6
5
4
3
2
1
0
-1
0
1000
2000
3000
4000
5000
6000
7000
8000
Time (s)

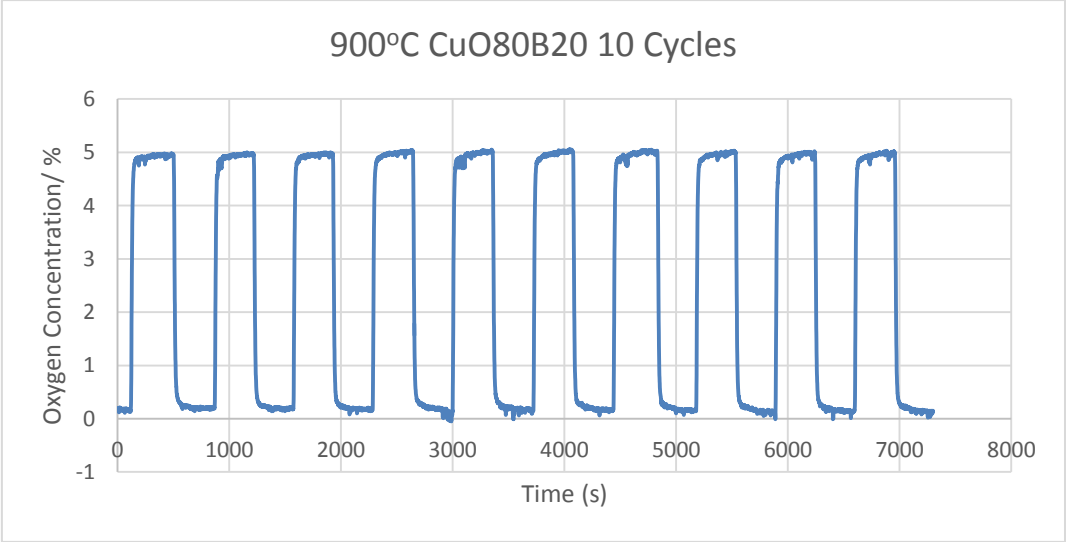
900°C CuO80B20 10 Cycles
Oxygen Concentration/ %
6
5
4
3
2
1
0
-1
0
1000
2000
3000
4000
5000
6000
7000
8000
Time (s)

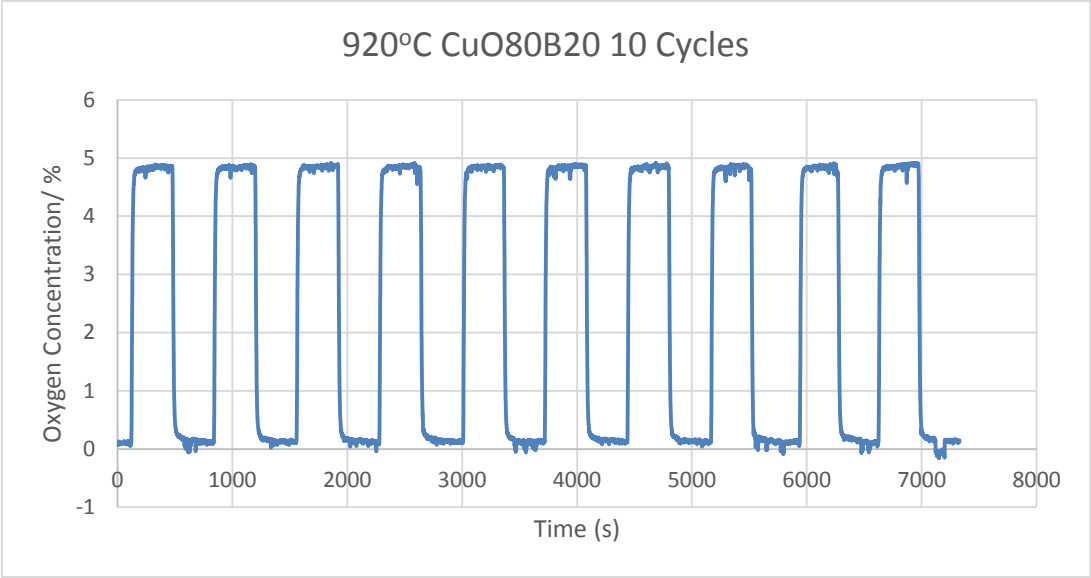
920°C CuO80B20 10 Cycles
Oxygen Concentration/ %
6
5
4
3
2
1
0
-1
0
1000
2000
3000
4000
5000
6000
7000
8000
Time (s)

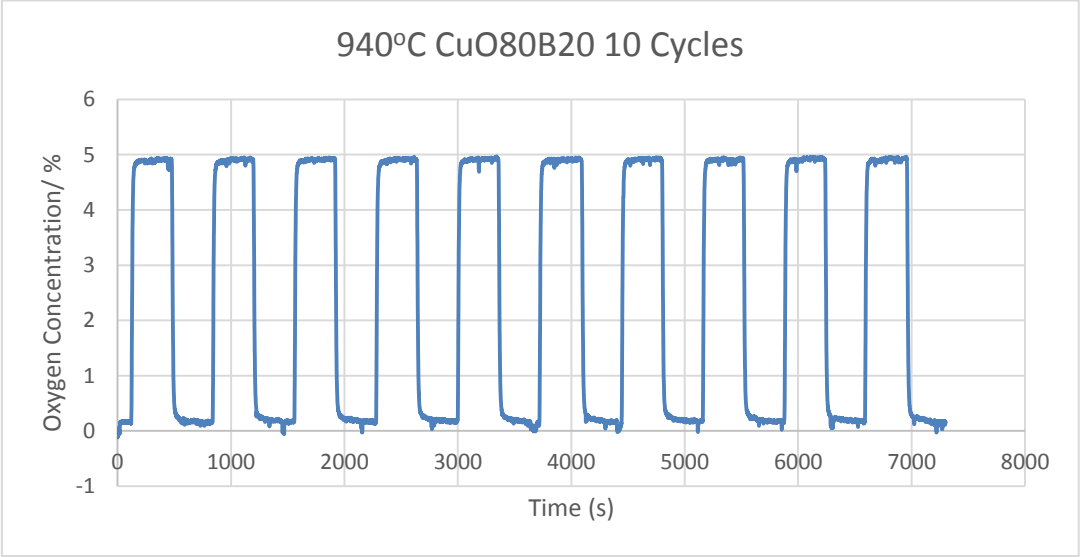
940°C CuO80B20 10 Cycles
Oxygen Concentration/ %
6
5
4
3
2
1
0
-1
0
1000
2000
3000
4000
5000
6000
7000
8000
Time (s)

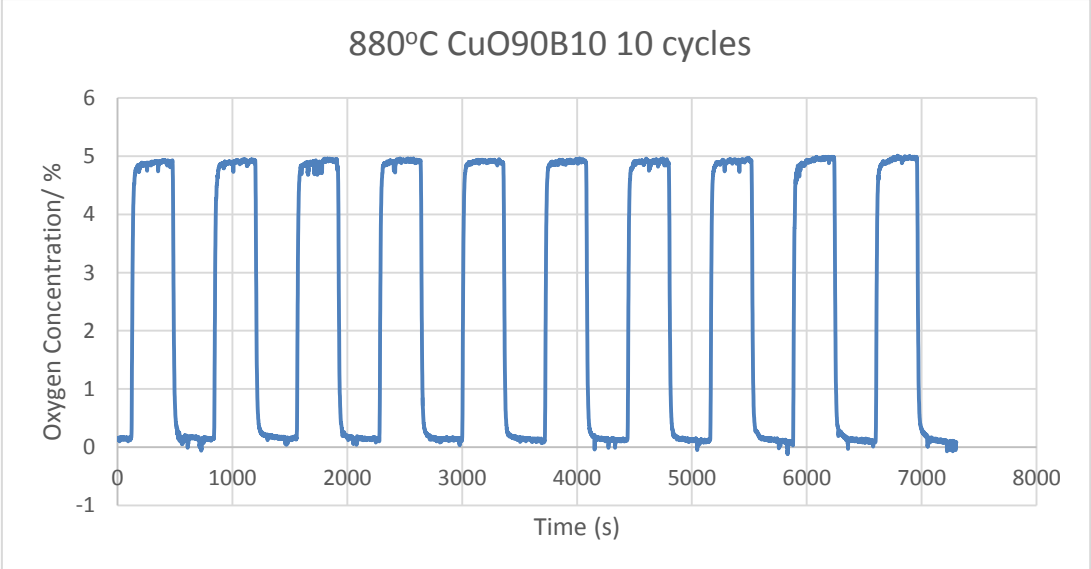
880°C CuO90B10 10 cycles
Oxygen Concentration/ %
6
5
4
3
2
1
0
-1
0
1000
2000
3000
4000
5000
6000
7000
8000
Time (s)

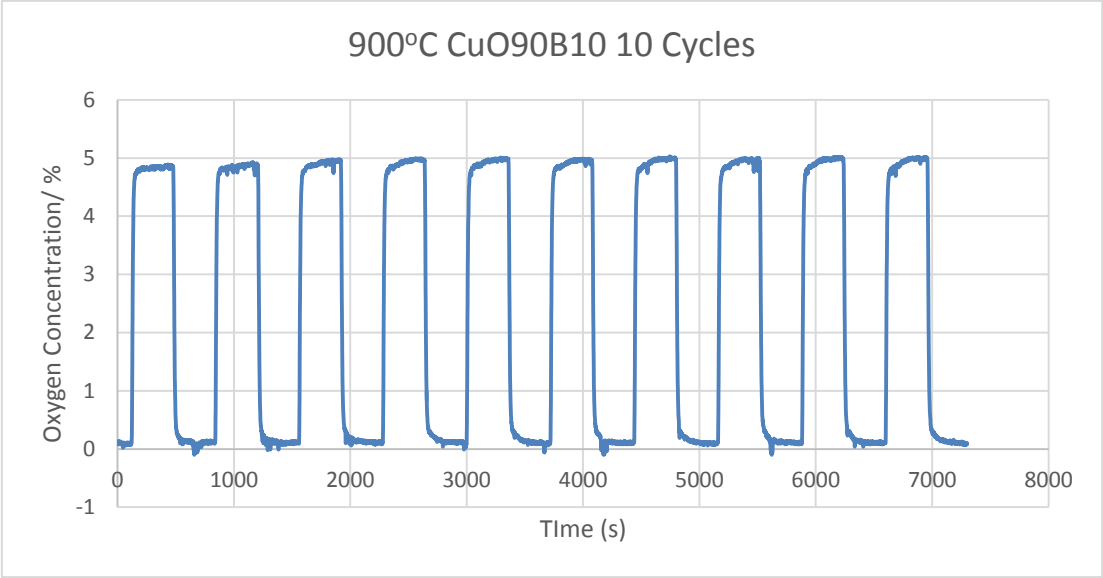
900°C CuO90B10 10 Cycles
Oxygen Concentration/ %
6
5
4
3
2
1
0
-1
0
1000
2000
3000
4000
5000
6000
7000
8000
TIme (s)

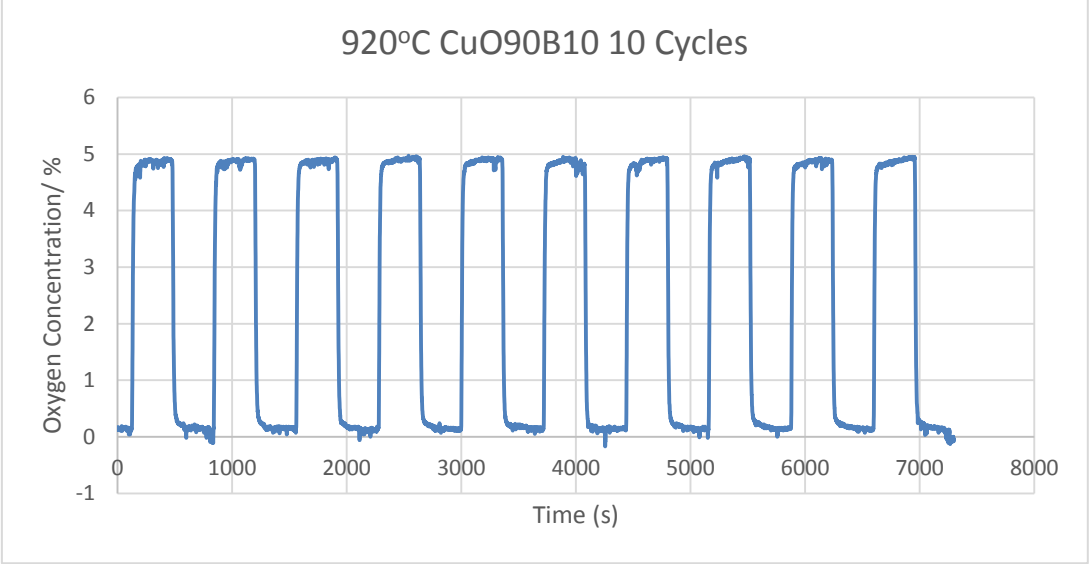
920°C CuO90B10 10 Cycles
Oxygen Concentration/ %
6
5
4
3
2
1
0
-1
0
1000
2000
3000
4000
5000
6000
7000
8000
Time (s)

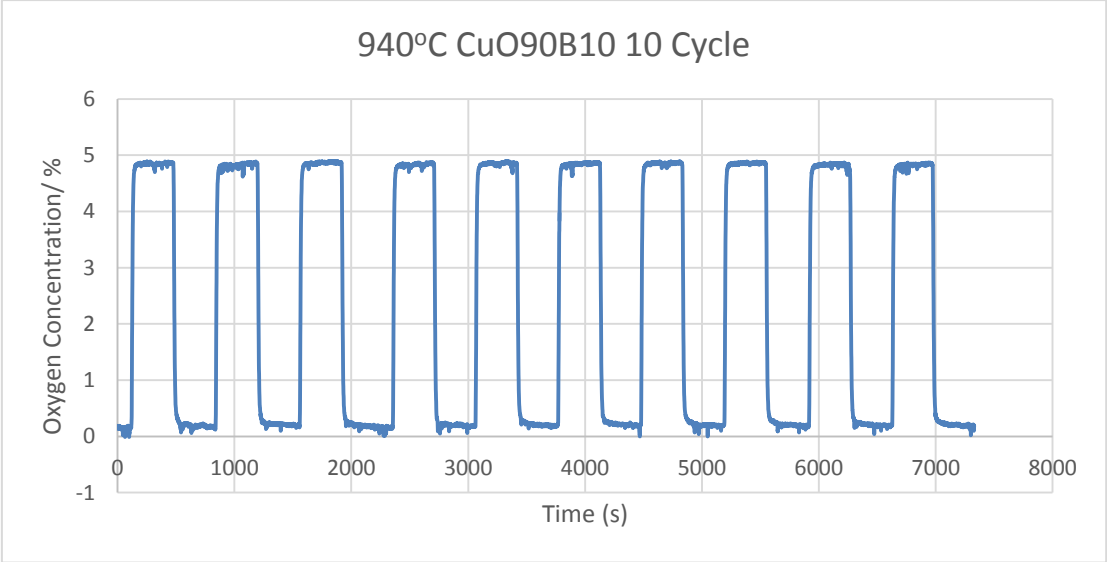
940°C CuO90B10 10 Cycle
Oxygen Concentration/ %
6
5
4
3
2
1
0
-1
0
1000
2000
3000
4000
5000
6000
7000
8000
Time (s)

Appendix 2 TGA Data

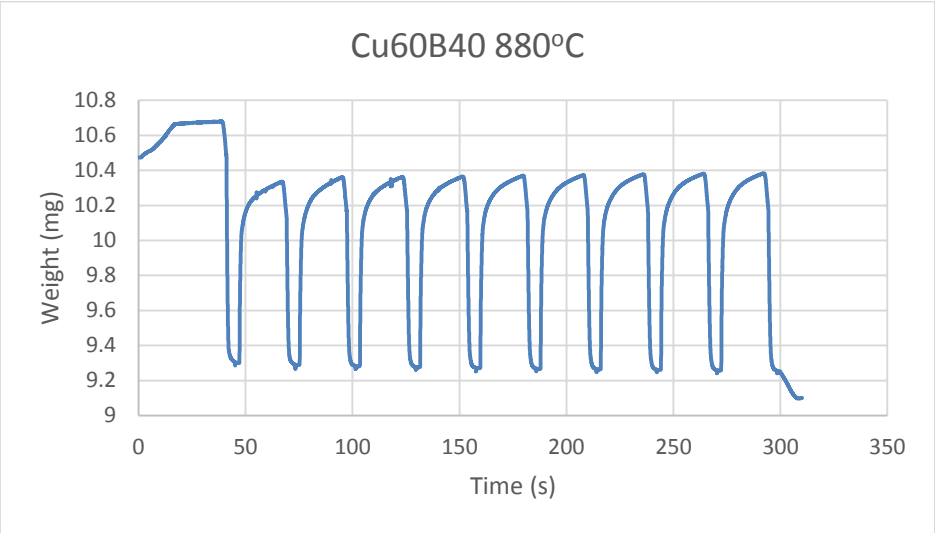

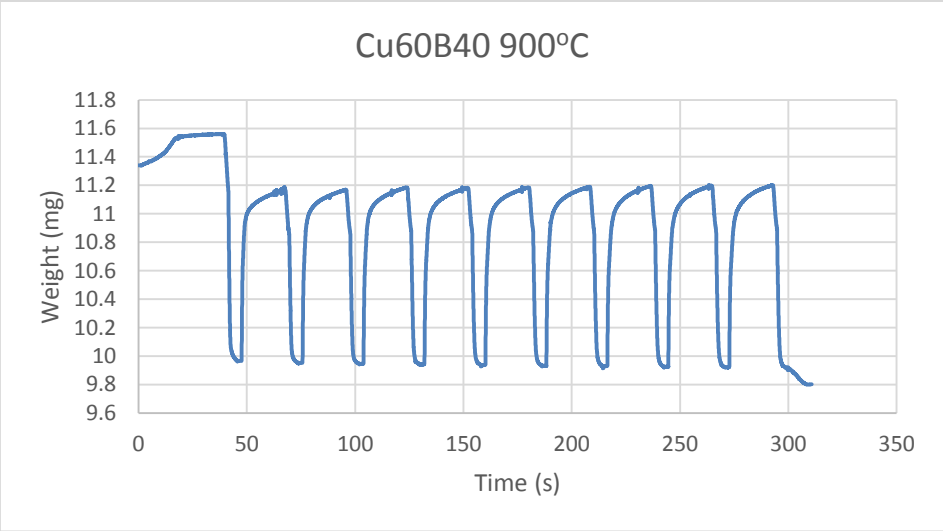

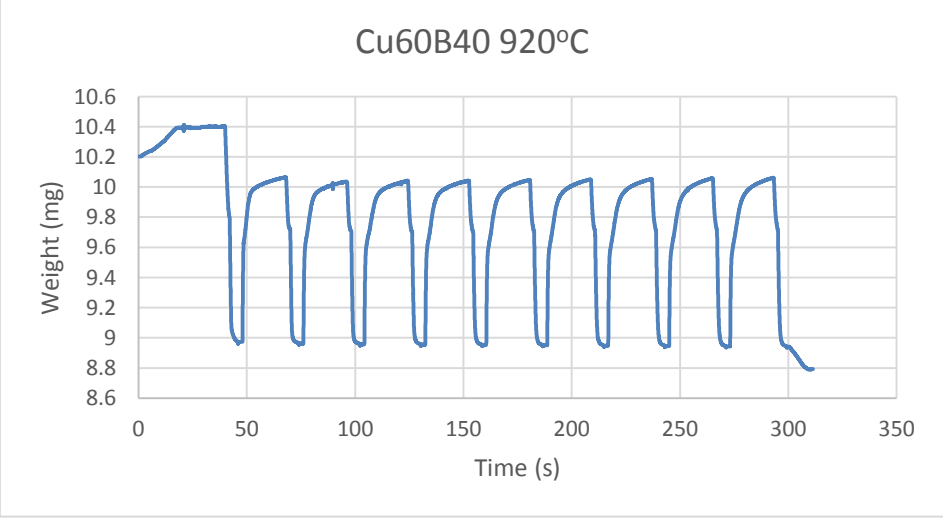

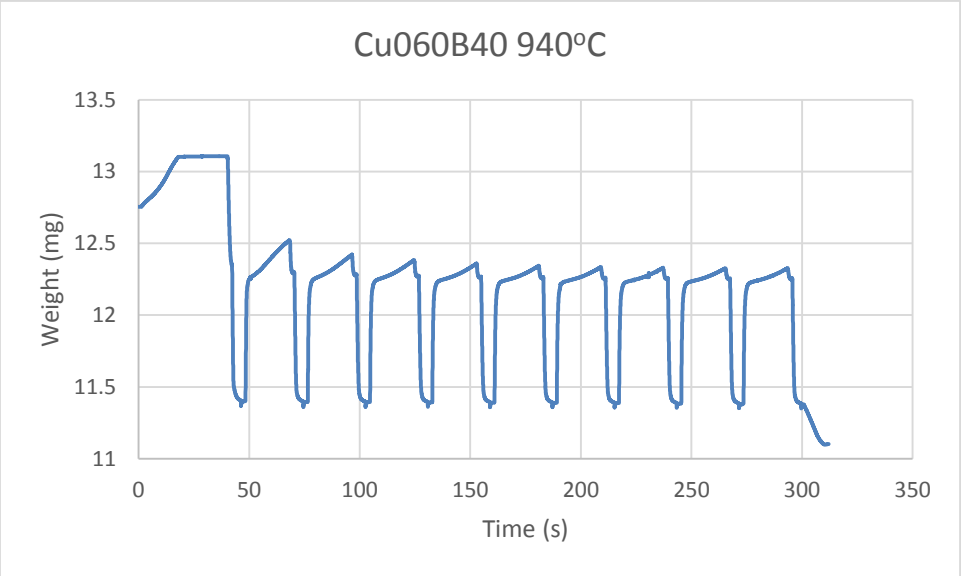
Cu060B40 940°C
Weight (mg)
13.5
13
12.5
12
11.5
11
0
50
100
150
200
250
300
350
Time (s)

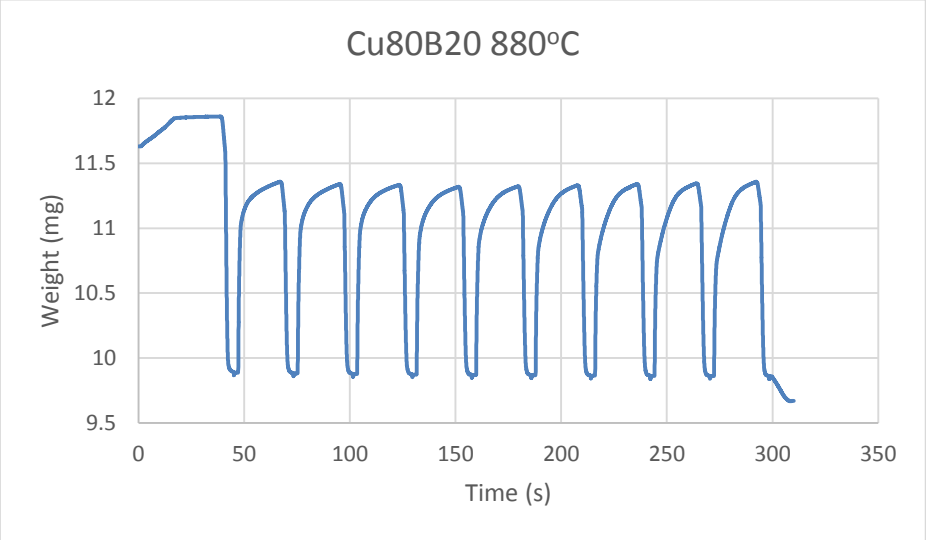
Cu80B20 880°C
Weight (mg)
12
11.5
11
10.5
10
9.5
0
50
100
150
200
250
300
350
Time (s)

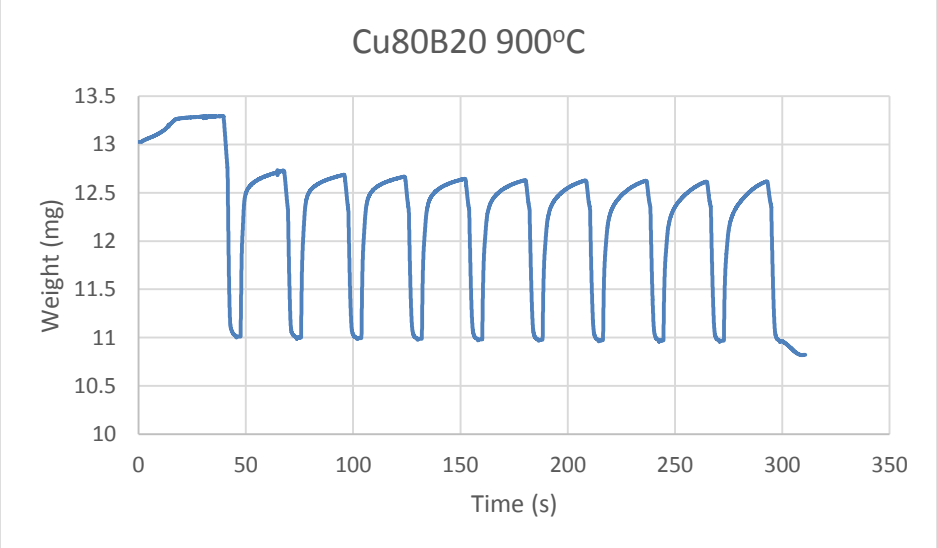
Cu80B20 900°C
Weight (mg)
13.5
13
12.5
12
11.5
11
10.5
10
0
50
100
150
200
250
300
350
Time (s)

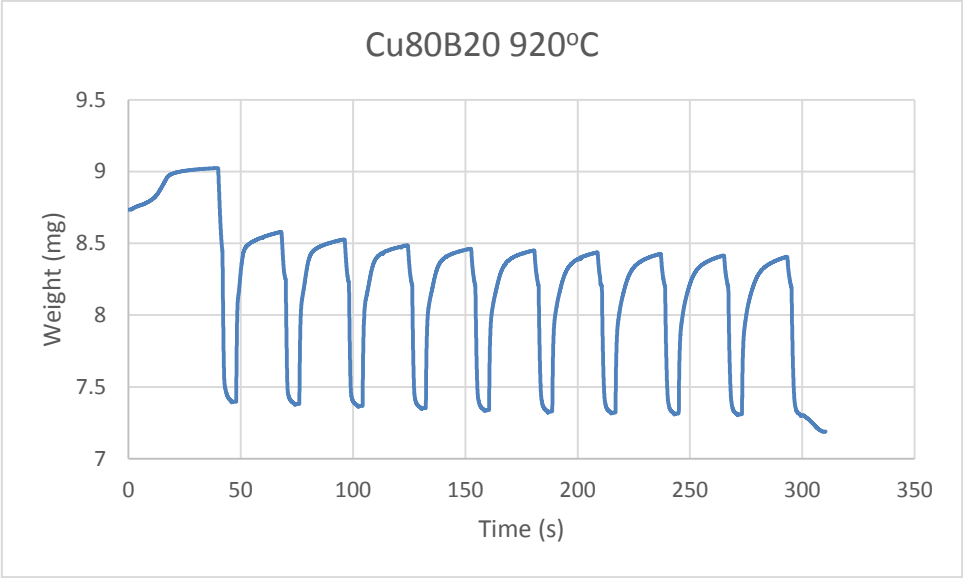
Cu80B20 920°C
Weight (mg)
9.5
9
8.5
8
7.5
7
0
50
100
150
200
250
300
350
Time (s)

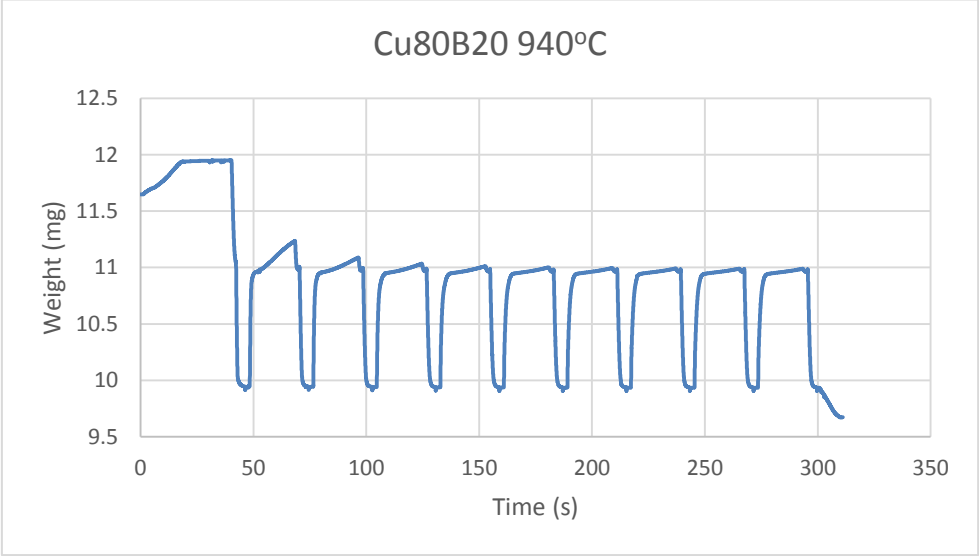
Cu80B20 940°C
Weight (mg)
12.5
12
11.5
11
10.5
10
9.5
0
50
100
150
200
250
300
350
Time (s)

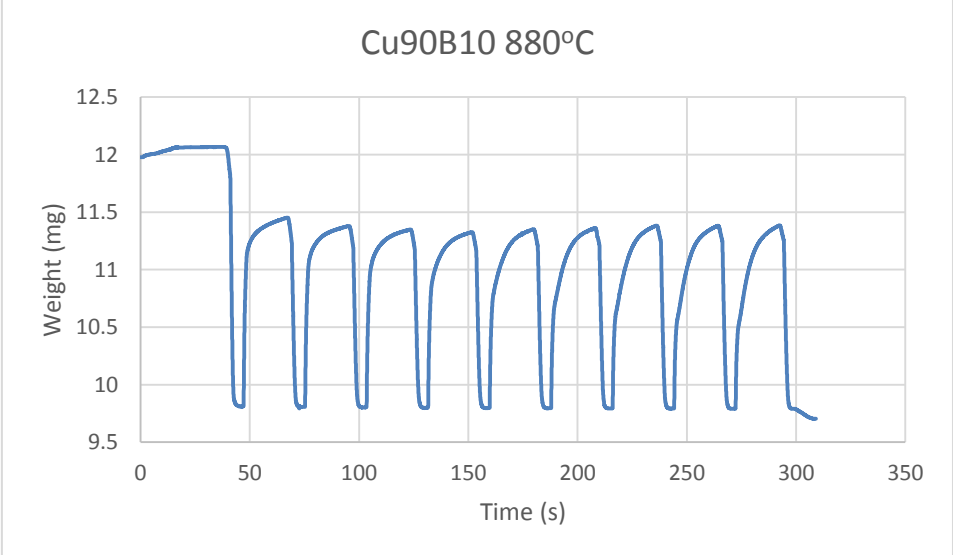
Cu90B10 880°C
Weight (mg)
12.5
12
11.5
11
10.5
10
9.5
0
50
100
150
200
250
300
350
Time (s)

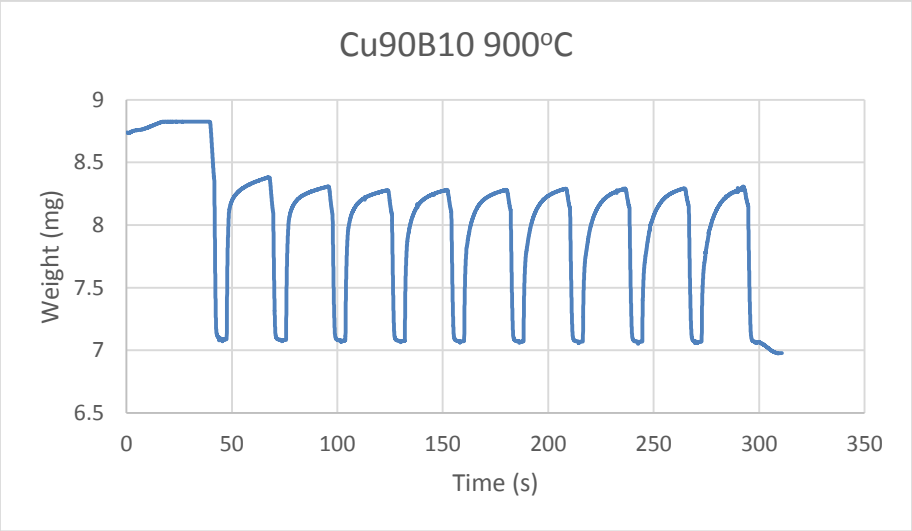
Cu90B10 900°C
Weight (mg)
9
8.5
8
7.5
7
6.5
0
50
100
150
200
250
300
350
Time (s)

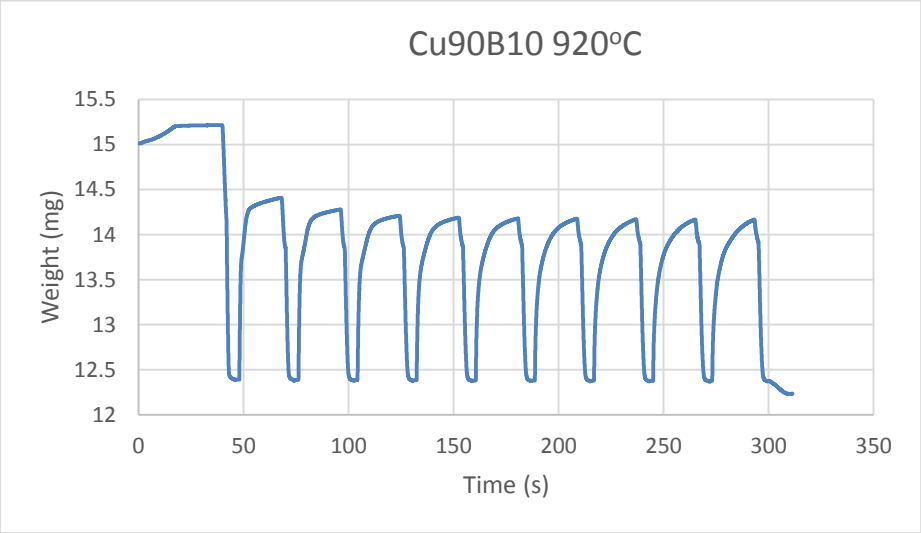
Cu90B10 920°C
Weight (mg)
15.5
15
14.5
14
13.5
13
12.5
12
0
50
100
150
200
250
300
350
Time (s)

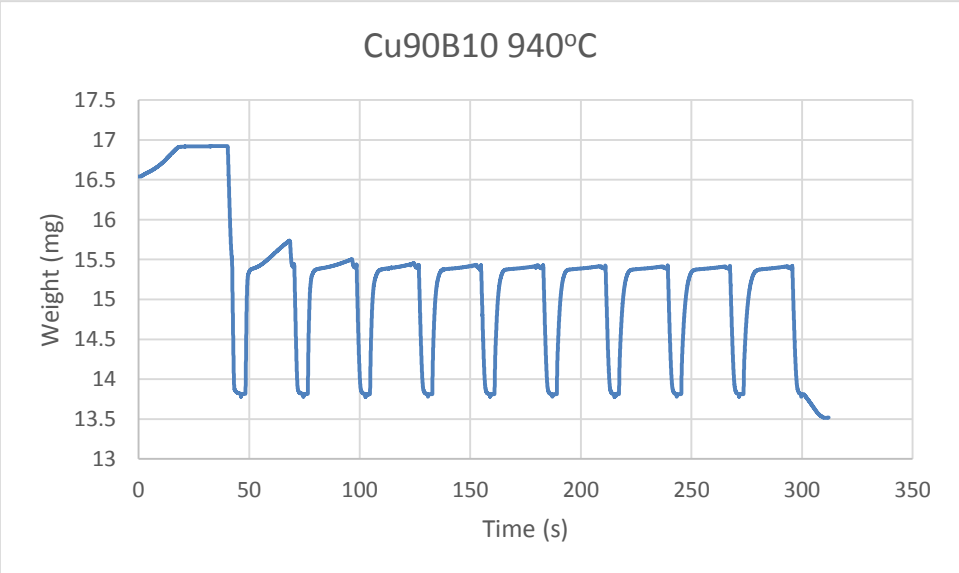
Cu90B10 940°C
Weight (mg)
17.5
17
16.5
16
15.5
15
14.5
14
13.5
13
0
50
100
150
200
250
300
350
Time (s)

Appendix 3 Oxidation Conversion in TGA Testing